Science Translational Medicine

AAAS

Make Your Research Hit the Target
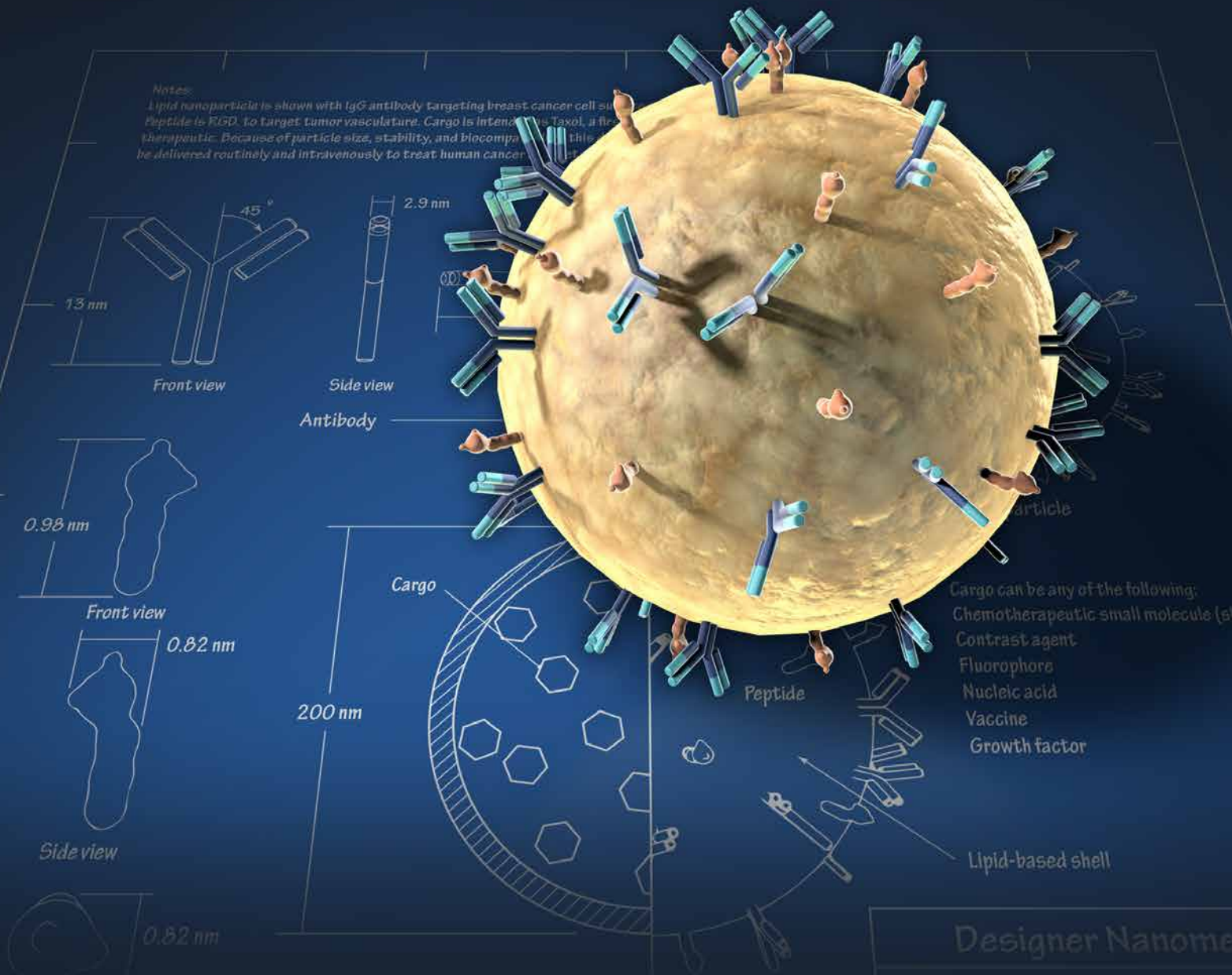
SPECIAL EDITION: Immunology
Select research published in *Science Translational Medicine*

The immune system is responsible for protecting our bodies from internal and external threats. Evolving knowledge about immunity can lead to life-saving treatments, such as CAR T cell therapy for cancer. The cover image shows two CAR T cells (blue) attacking a lymphoma cell (pink). *Science Translational Medicine* is a leading interdisciplinary journal that publishes biomedical translational research, including the cutting-edge immunology studies featured in this Special Edition.

Credit: STEVE GSCHMEISSNER/Science Source

Science Translational Medicine | AAAS

Science Translational Medicine is an interdisciplinary journal that publishes translational research with impact for human health that fills the knowledge gaps between preclinical studies and clinical applications.

Scientific Advisory Board

CANCER

MHC proteins confer differential sensitivity to CTLA-4 and PD-1 blockade in untreated metastatic melanoma

Scott J. Rodig[1,2]*, Daniel Gusenleitner[1], Donald G. Jackson[3], Evisa Gjini[1], Anita Giobbie-Hurder[4], Chelsea Jin[3], Han Chang[3], Scott B. Lovitch[2], Christine Horak[3], Jeffrey S. Weber[5], Jason L. Weirather[4], Jedd D. Wolchok[6], Michael A. Postow[6,7], Anna C. Pavlick[5], Jason Chesney[8], F. Stephen Hodi[9]*

Combination anti–cytotoxic T lymphocyte antigen 4 (CTLA-4) and anti–programmed cell death protein 1 (PD-1) therapy promotes antitumor immunity and provides superior benefit to patients with advanced-stage melanoma compared with either therapy alone. T cell immunity requires recognition of antigens in the context of major histocompatibility complex (MHC) class I and class II proteins by CD8$^+$ and CD4$^+$ T cells, respectively. We examined MHC class I and class II protein expression on tumor cells from previously untreated melanoma patients and correlated the results with transcriptional and genomic analyses and with clinical response to anti–CTLA-4, anti–PD-1, or combination therapy. Most (>50% of cells) or complete loss of melanoma MHC class I membrane expression was observed in 78 of 181 cases (43%), was associated with transcriptional repression of *HLA-A*, *HLA-B*, *HLA-C*, and *B2M*, and predicted primary resistance to anti–CTLA-4, but not anti–PD-1, therapy. Melanoma MHC class II membrane expression on >1% cells was observed in 55 of 181 cases (30%), was associated with interferon-γ (IFN-γ) and IFN-γ–mediated gene signatures, and predicted response to anti–PD-1, but not anti–CTLA-4, therapy. We conclude that primary response to anti–CTLA-4 requires robust melanoma MHC class I expression. In contrast, primary response to anti–PD-1 is associated with preexisting IFN-γ–mediated immune activation that includes tumor-specific MHC class II expression and components of innate immunity when MHC class I is compromised. The benefits of combined checkpoint blockade may be attributable, in part, to distinct requirements for melanoma-specific antigen presentation to initiate antitumor immunity.

INTRODUCTION

Patients with advanced melanoma derive greater benefit from combined treatment with antibodies targeting cytotoxic T lymphocyte antigen 4 (CTLA-4) and programmed cell death protein 1 (PD-1) than from either antibody alone (*1*, *2*). However, the shared and unique biological effects derived from inhibiting the two immune checkpoint proteins are still poorly understood. In vitro and preclinical models show that CTLA-4, expressed by T cells, binds members of the B7 family expressed by antigen-presenting cells (APCs) to inhibit T cell costimulation during the priming and effector phases of T cell activation (*3*, *4*). PD-1, expressed by activated T cells, binds the PD-1 ligands expressed by tumors and APCs to inhibit T cell effector function, a reversible phenotype termed "exhaustion" (*5*, *6*). Combined CTLA-4 and PD-1 blockade relieves both inhibitors of T cell activity and generally results in superior antitumor activity compared with either therapy alone (*7*–*9*). However, antitumor immune responses remain dependent on T cell recognition of tumor-specific antigens in the context of major histocompatibility complex (MHC) proteins to affect tumor regression (*10*–*12*).

Validation of these mechanisms of action in patients treated with therapeutic anti–CTLA-4 and anti–PD-1 antibodies is ongoing. There are presently no cellular or protein biomarkers predictive of response to anti–CTLA-4 treatment. In contrast, the presence of a T cell infiltrate, PD-1$^+$ immune cells, and programmed cell death ligand 1–positive (PD-L1$^+$) inflammatory and tumor cells in pretreatment biopsy samples are indicators of ongoing but exhausted antitumor immunity and predict better clinical response and overall patient survival with anti–PD-1 treatment (*13*–*18*). Tumors with a high burden of somatic mutations are also associated with better outcomes among patients treated with anti–CTLA-4 or anti–PD-1 therapy, presumably because of an increased number of neopeptide antigens presented by tumor cells to T cells in the context of MHC (*19*–*21*).

Emerging data suggest that reduction or loss of proteins associated with antigen presentation can be a mechanism to evade antitumor immunity after immune checkpoint blockade (*22*). However, the prevalence and significance of altered antigen presentation remain incompletely characterized. We evaluated the expression of MHC class I and class II proteins in pretreatment biopsy samples from patients treated with ipilimumab (IPI; anti–CTLA-4) followed by nivolumab (NIVO; anti–PD-1) (IPI→NIVO), NIVO followed by IPI (NIVO→IPI), IPI alone, or concurrent NIVO + IPI in the clinical trial setting. The results were correlated with transcriptional and genomic profiles available for a subset of the cases and with clinical outcomes.

RESULTS

Expression of MHC proteins in untreated melanoma

Pretreatment biopsies analyzed by immunohistochemistry (IHC) with an antibody recognizing all classical MHC class I proteins revealed positive membrane staining of all cells in normal skin,

[1]Center for Immuno-Oncology, Dana-Farber Cancer Institute, Boston, MA 02215, USA. [2]Department of Pathology, Brigham and Women's Hospital, Boston, MA 20115, USA. [3]Bristol-Myers Squibb, Princeton, NJ 08540, USA. [4]Department of Biostatistics and Computational Biology, Dana-Farber Cancer Institute, Boston, MA 02215, USA. [5]Laura and Isaac Perlmutter Cancer Center, New York University Langone Medical Center, New York, NY 10016, USA. [6]Melanoma and Immunotherapeutics Service, Department of Medicine, Memorial Sloan Kettering Cancer Center, New York, NY 10065, USA. [7]Department of Medicine, Weill Cornell Medical College, New York, NY 10065, USA. [8]James Graham Brown Cancer Center, University of Louisville, Louisville, KY 40202, USA. [9]Melanoma Disease Center, Dana-Farber Cancer Institute, Boston, MA 02215, USA.
*Corresponding author. Email: srodig@bwh.harvard.edu (S.J.R.); stephen_hodi@dfci.harvard.edu (F.S.H.)

Fig. 1. Summary of MHC class I and MHC class II data from the CheckMate 064 trial. MHC class I and MHC class II expression is shown in melanoma biopsy samples. (**A**) Double chromogenic IHC with antibodies targeting SOX10 (red coloration) and MHC class I (i, iii, v; brown coloration) in representative cases showing membrane staining of all SOX10^{+} melanoma cells (i), subset of melanoma cells (iii, scored as 50% tumor cell–positive), and no melanoma cell–positive (v; yellow arrow indicates PAX5-negative lymphocyte with positive membrane staining), or SOX10 (red coloration) and MHC class II (ii, iv, vi; brown coloration) in representative cases showing positive membrane staining MHC class II in all SOX10^{+} melanoma cells (ii) and no melanoma cell–positive (iv and vi; yellow arrow in iv indicates PAX5-negative lymphocyte with positive membrane staining). (**B**) Heat map representing the positive membrane staining of tumor cells (0 to 100%) for MHC class I (row 1) and MHC class II (row 2) proteins, the relative RNA expression of *HLA-A*, *HLA-B*, and *HLA-C* (rows 3 to 5, respectively), and the presence and type of alterations in *HLA*, *B2M*, *STAT1*, *JAK2*, and *JAK1* genes (rows 6 to 10, respectively) for all cases (columns) with available data in the series. The threshold of 50% of tumor cells positive for MHC class I is indicated (red arrow and line). HLA, human leukocyte antigen; CN, copy number. (**C** to **F**) Kaplan-Meier estimates of overall survival (OS) by MHC class I and MHC class II expression in baseline biopsy samples according to treatment arms. OS according to expression of MHC class I is divided according to the optimum (50%) for the IPI→NIVO arm (C; *P* = 0.01) and the NIVO→IPI arm (D; *P* = 0.46). OS according to the expression of MHC class II is divided according to the optimum (1%) for the IPI→NIVO arm (E; *P* = 0.14) and the NIVO→IPI arm (F; *P* = 0.01). Patients with incomplete biomarker data are indicated (solid gray lines). Vertical dashed lines indicate the two critical time points for this analysis: 13 weeks (point of therapy switch) and 25 weeks (initiation of maintenance NIVO). The number of evaluated at-risk patients was 42 for the IPI→NIVO arm and 50 for the NIVO→IPI arm. Median OS (in months) and the HR for OS, with the 95% CIs for each, are listed below the curves. NR, not reached.
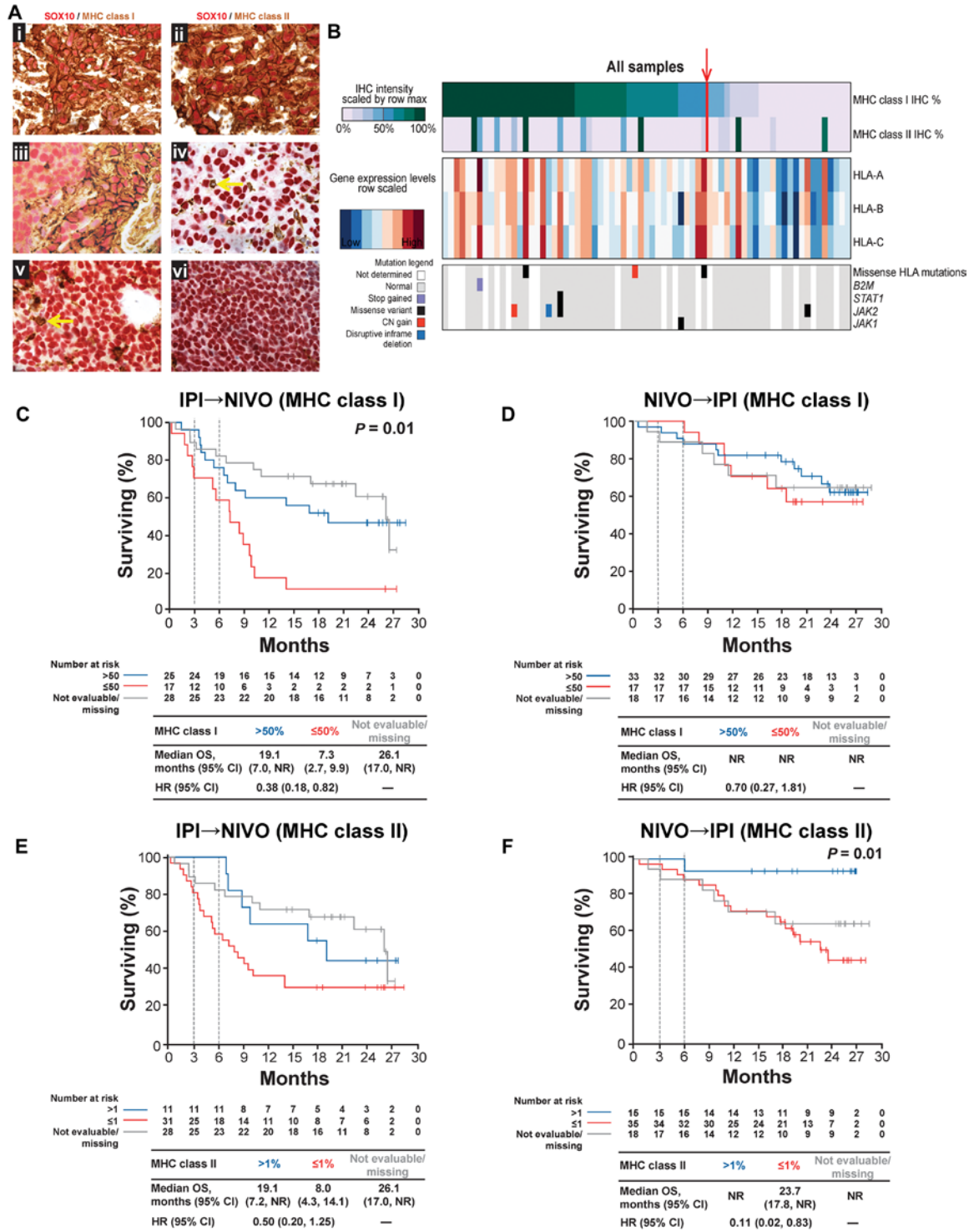
including SOX10^{+} melanocytes (fig. S1A). IHC performed on biopsy samples from patients with advanced-stage melanoma enrolled in CheckMate 064 revealed variable expression of MHC class I proteins on SOX10^{+} melanoma cells compared with nonmalignant cells within the same tissue before immunotherapy (Fig. 1, A and B, fig. S1, and table S1). Malignant cells lacking membrane staining included those with only cytoplasmic staining and those with no staining. Membrane MHC class I expression on melanoma cells ranged from 100 to 0% (median, 70%). Lack of MHC class I expression on most of malignant cells (>50%) was observed in 34 of 92 cases (37%; Fig. 1B).

The percentages of melanoma tumor cells with MHC class I protein expression correlated with the percentages of tumor cells displaying the independently assessed protein biomarker β-2-microglobulin (β2M) ($\rho = 0.74$; $P < 0.001$; nonmalignant cells served as an internal positive control for β2M staining; fig. S2A). The distribution of IHC scores for MHC class I and β2M suggested that IHC for MHC class I was more sensitive than IHC for β2M for detecting positive membrane staining and was therefore used for subsequent analyses (fig. S2A). Reduced amounts of MHC class I protein expression on melanoma cells were also associated with reduced amounts of the MHC class I transcripts *HLA-A*, *HLA-B*, and *HLA-C* in the bulk population ($P = 0.007$, Wilcoxon rank sum test; Fig. 1B and fig. S2B). Reduced *HLA-A*, *HLA-B*, and *HLA-C* transcripts further correlated with reduced *B2M* transcripts across samples ($\rho = 0.8$ to 0.87; $P < 0.001$), consistent with coordinately reduced transcriptional expression of these MHC class I pathway components.

A stop codon in the coding region of *B2M* was observed at a low allele frequency (6%) for one case with positive membrane staining for MHC class I and β2M proteins in >90% of melanoma cells (Fig. 1B). There were no mutations in the *HLA-A*, *HLA-B*, *HLA-C*, or *B2M* genes that could explain reduced MHC class I transcript and protein expression in additional cases. Interferon-γ (IFN-γ)–mediated Janus kinase (JAK)–signal transducer and activator of transcription (STAT) signaling is a potent regulator of MHC class I and class II expression, and somatic mutations have been reported in *JAK1* and *JAK2* in a small number of tumors resistant to immunotherapy (22). We found a disruptive in-frame deletion in *JAK2* at low frequency (4%) in one case with MHC class I protein expression in >90% of cells (Fig. 1B). There were no mutations in *JAK1*, *JAK2*, or *STAT1* that could explain reduced MHC class I transcript and protein expression in additional cases. Together, these data indicate that most or complete loss of MHC class I/β2M protein expression, likely attrib-

utable to transcriptional down-regulation of *HLA* and *B2M* genes, is common in advanced melanomas before immunotherapy.

IHC performed with an antibody recognizing all classical MHC class II proteins revealed positive membrane staining of cells morphologically consistent with Langerhans cells in normal skin, but no staining of SOX10^{+} melanocytes or keratinocytes (fig. S1K). More than 1% of melanoma cells expressed membrane MHC class II in 26 of 92 cases (28%) from CheckMate 064 (Fig. 1, A and B, and table S1). In contrast to MHC class I, the percentage of malignant cells with positive staining for MHC class II was generally very low (median, 10%; range, 1 to 100%) and was concentrated at the inflammatory invasive margin of the tumor, consistent with induced local expression (fig. S1, L to N).

MHC protein expression and response to checkpoint blockade in CheckMate 064

We next examined whether tumor MHC class I or MHC class II expression in pretreatment biopsy samples was associated with disease progression with single-agent IPI or single-agent NIVO at week 13, the time of therapy switch, for patients enrolled in CheckMate 064 (fig. S3A shows the trial schematic). Reduced tumor MHC class I expression (≤30%) identified patients who are more likely to have progressive disease than complete response, partial response, or stable disease at week 13 after single-agent IPI ($P = 0.02$, Fisher's exact test; Table 1). No amount of MHC class I expression distinguished patients with from those without progressive disease at week 13 after single-agent NIVO (Table 1). Conversely, MHC class II expression (>1%) associated with patients who are more likely to have complete or partial responses or stable disease than progressive disease at week 13 after single-agent NIVO, although the P value was just outside the range of statistical significance ($P = 0.0517$, Fisher's exact test; Table 1). No amount of tumor MHC class II expression distinguished patients with complete responses, partial responses, or stable disease from those with progressive disease at week 13 after single-agent IPI (Table 1). Given that single-agent therapy for each arm of the study was of limited duration (13 weeks), we did not further subdivide the response assessment (that is, into complete/partial response and stable disease) for these comparisons. The results were highly significant when best overall response for the trial was also considered ($P = 0.03$ for MHC class I in IPI→NIVO, $P = 0.005$ for MHC class II in NIVO→IPI; Fisher's exact test; table S2).

For a small set of patients, matched baseline and week 13 biopsy samples were available for comparison ($n = 10$ for IPI, $n = 11$ for

Table 1. Progressive disease at week 13 according to MHC class I and MHC class II thresholds in CheckMate 064.

Biomarker	Optimal threshold (%)	Number of patients			Proportion with low biomarker expression and PD	Proportion with high biomarker expression and PD	Fisher's exact P value
		In analysis	Low expression	High expression			
IPI							
MHC class I	30	42	14	28	1.00	0.64	0.02
MHC class II	50	42	41	1	0.76	1.00	0.99
NIVO							
MHC class I	30	50	16	34	0.44	0.32	0.53
MHC class II	1	50	35	15	0.46	0.13	0.05

NIVO; fig. S4). We did not observe changes in MHC class I or MHC class II expression status (high versus low) between baseline and week 13 samples among patients treated with IPI. We observed changes in MHC class I and/or class II status between baseline and week 13 samples for a minority of patients treated with NIVO (4 of 11), but we found no strict correlation between those patients' status at week 13 and progressive disease (fig. S4).

When overall survival was examined, low baseline tumor MHC class I expression (≤50%) was associated with inferior overall survival for patients initially treated with IPI, despite an eventual exposure to NIVO for patients continuing in the trial [IPI→NIVO treatment arm; hazard ratio (HR), 0.38; 95% confidence interval (CI), 0.18 to 0.82; $P = 0.01$; Fig. 1C]. No amount of tumor MHC class I expression, including the 50% threshold (HR, 0.70; 95% CI, 0.27 to 1.18; $P = 0.46$), identified a population with inferior overall survival when initially treated with NIVO (Fig. 1D). Conversely, baseline tumor MHC class II expression (>1%) was associated with better overall survival for patients initially treated with NIVO, despite eventual exposure to IPI for patients continuing in the trial (NIVO→IPI arm; HR, 0.11; 95% CI, 0.02 to 0.83; $P = 0.01$; Fig. 1F). No amount of tumor MHC class II expression, including the 1% threshold (HR, 0.50; 95% CI, 0.20 to 1.25; $P = 0.14$), reached statistical significance for predicting the overall survival of patients initially treated with IPI (Fig. 1E).

MHC protein expression and response to checkpoint blockade in CheckMate 069

To validate the associations between melanoma MHC class expression and survival in a distinct cohort, we evaluated baseline biopsy samples from treatment-naïve patients treated with single-agent IPI (with the option of NIVO at disease progression) or concurrent NIVO + IPI while enrolled in CheckMate 069 (fig. S3B shows the study schematic). Lack of MHC class I expression on most of malignant cells (>50%) was observed in 44 of 89 cases (49%; Fig. 2, A and B, and table S3). More than 1% of melanoma cells expressed membrane MHC class II in 29 of 89 cases (33%) from CheckMate 069 (Fig. 2, C and D). Among patients treated with single-agent IPI ($n = 26$), reduced tumor MHC class I expression [at the previously defined optimal threshold for overall survival in CheckMate 064 (≤50%)] was associated with a best overall response of progressive disease ($P = 0.01$; Table 2). Given that most patients received a defined therapy for the course of the trial, we further subdivided the best overall responses according to clinical nonresponse (progressive or stable disease) versus response (complete or partial response) for comparison. Reduced tumor MHC class I expression perfectly predicted a lack of clinical response to IPI (negative predictive value, 100%; 95% CI, 74 to 100%; Table 2). Although the P value was outside the range of significance ($P = 0.057$; Fig. 2A), reduced MHC class I (≤50%) was additionally associated with inferior overall survival after IPI treatment, with visible separation of the Kaplan-Meier curves (Fig. 2A), and an HR (0.34; 95% CI, 0.11 to 1.03) nearly identical to that found for patients initially treated with IPI in CheckMate 064 (Fig. 1C). Among patients treated with concurrent NIVO + IPI ($n = 63$), reduced MHC class I expression was not associated with progressive disease, inferior response, or inferior overall survival (Table 2 and Fig. 2B). Positive tumor MHC class II expression, which was associated with superior overall survival among patients initially treated with single-agent NIVO before single-agent IPI in CheckMate 064 (Fig. 1F),

did not identify a group with superior clinical response or superior overall survival among patients treated with single-agent IPI or concurrent NIVO + IPI in CheckMate 069 (Table 2 and Fig. 2, C and D). Thus, these data suggest that robust tumor-specific MHC class I expression is essential for response to anti–CTLA-4 therapy but not to anti–PD-1 or combination therapy, whereas tumor-specific MHC class II expression is associated with superior response to anti–PD-1 therapy, but not to anti–CTLA-4 or combination therapy.

Transcriptional signatures of response to checkpoint blockade in CheckMate 064

To better define the immunological criteria for response to immune checkpoint blockade, we analyzed RNA sequencing (RNA-seq) data from freshly frozen biopsy samples obtained during CheckMate 064. A 10-gene IFN-γ–related transcriptional signature (table S4), previously suggested as predictive of response to the anti–PD-1 agent pembrolizumab (23), was significantly higher in baseline biopsy samples from patients without progressive disease compared to those with progressive disease at week 13 after single-agent NIVO ($P = 0.03$, Wilcoxon rank sum test; Fig. 3A). This association was not observed among patients treated with single-agent IPI ($P = 0.18$, Wilcoxon rank sum test; Fig. 3A). Similarly, the IFN-γ signature was significantly higher in baseline biopsy samples from patients without progressive disease (complete response, partial response, and stable disease) as best overall response compared with patients with progressive disease in the NIVO→IPI arm of the trial ($P = 0.003$, Wilcoxon rank sum test; Fig. 3B). This association was not observed among patients in the IPI→NIVO arm ($P = 0.20$, Wilcoxon rank sum test; Fig. 3B).

To independently uncover the immunological determinants of immunotherapy response, we examined the RNA-seq data for 770 immune-associated genes and identified the top 25 differentially expressed gene transcripts associated with a lack of progressive disease as the best overall patient response in patients receiving NIVO before IPI in CheckMate 064 (Fig. 3C). Thirteen of the top 25 immune transcripts were directly related to IFN-γ (Fig. 3C). These included a cytokine (*IFNG*), a transcription factor associated with IFN-γ production [*TBX21* (*Tbet*)], markers of adaptive and innate immune cells responsible for IFN-γ production (*CD8A*, *TIGIT*, and *KLRD1*), and major gene targets of IFN-γ–mediated signaling (Fig. 3C) (24–26). Six genes identified by this method were shared with the independently discovered, pembrolizumab-derived gene signature (table S4).

We found that a gene set score derived from the top 25 differentially expressed genes was significantly higher in baseline biopsy samples from patients without progressive disease compared with those with progressive disease at week 13 after single-agent NIVO, as expected ($P = 0.004$, Wilcoxon rank sum test; Fig. 3A). However, we did not find this association among patients receiving single-agent IPI ($P = 0.26$, Wilcoxon rank sum test; Fig. 3A). In addition, we found that a distilled 13-gene IFN-γ–related gene set score was significantly higher in baseline biopsy samples from patients without progressive disease compared with those with progressive disease at week 13 after single-agent NIVO ($P = 0.01$, Wilcoxon rank sum test; Fig. 3A). We did not find this association among patients receiving single-agent IPI ($P = 0.24$, Wilcoxon rank sum test; Fig. 3A). We found similar results when the best overall response of nonprogressive disease versus progressive disease for the full trial was used as an end point (Fig. 3B).
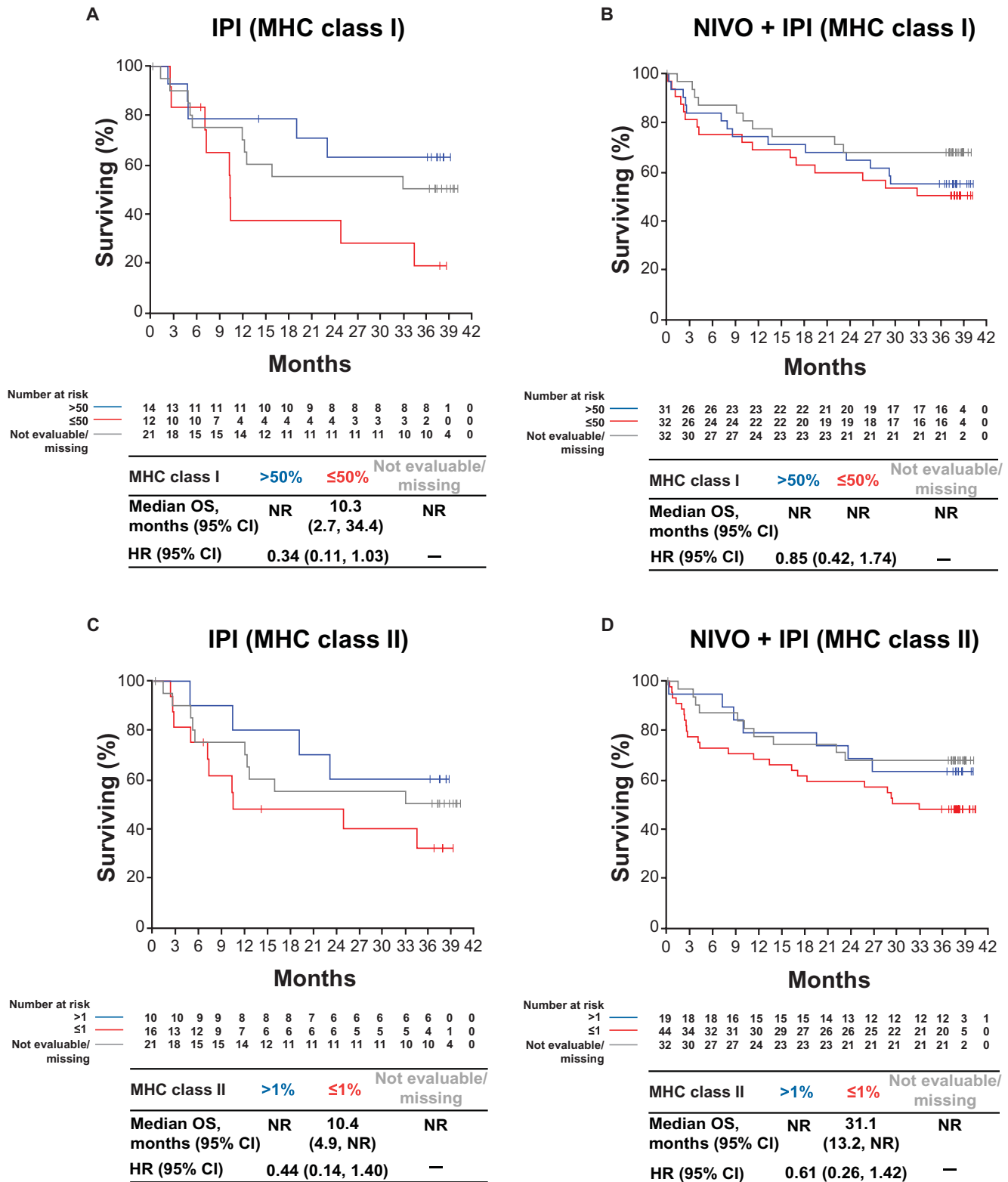
Fig. 2. Summary of MHC class I and MHC class II data from the CheckMate 069 trial. Kaplan-Meier estimates of OS by MHC class I and MHC class II expression in baseline biopsy samples according to treatment arm are shown. OS was divided according to the determined threshold for MHC class I (50%) in the (**A**) IPI arm ($P = 0.057$) and (**B**) NIVO + IPI arm ($P = 0.66$). OS was also divided according to the determined threshold for MHC class II (1%) in the (**C**) IPI arm ($P = 0.16$) and (**D**) NIVO + IPI arm ($P = 0.25$). The number of evaluated at-risk patients was 26 for the IPI arm and 63 for the NIVO + IPI arm. The median OS (in months) and the HR, with 95% CIs for each, are listed below the curves.

Table 2. Disease progression according to defined biomarker thresholds in CheckMate 069. NPV, negative predictive value; PPV, positive predictive value.

Biomarker	Threshold (%)	Number of patients			Proportion with low biomarker expression and PD	Proportion with high biomarker expression and PD	Fisher's exact P value	Predictive values (response* versus nonresponse)	
		In analysis	Low expression	High expression				NPV (95% exact CI)	PPV (95% exact CI)
IPI									
MHC class I	50	26	12	14	0.92	0.43	0.01	100% (74–100%)	21% (5–51%)
MHC class II	1	26	16	10	0.75	0.50	0.23	94% (70–99%)	20% (3–56%)
NIVO + IPI									
MHC class I	50	63	32	31	0.31	0.29	0.99	41% (24–59%)	55% (36–73%)
MHC class II	1	63	44	19	0.36	0.16	0.14	50% (35–65%)	74% (49–91%)

*Defined as complete response or partial response.

IFN-γ is produced by activated T cells and natural killer (NK) cells and directly and potently induces MHC class II expression on tumor and immune cells (26). The predictive power of baseline IFN-γ transcriptional signatures suggested a biological link between IFN-γ and the focal melanoma MHC class II expression that we observed at the inflammatory margin for a subset of tumors. Consistent with this, we observed a positive correlation between our empirically derived IFN-γ gene set score and baseline melanoma MHC class II protein expression across all samples (Kendall's pairwise correlation τ = 0.43, $P < 0.001$; Fig. 3D). The magnitudes of our IFN-γ gene set score and the previously published IFN-γ signature were positively correlated with the number of tumor-associated CD3$^+$, CD4$^+$, and CD8$^+$ T cells, known sources of IFN-γ, and with melanoma PD-L1 expression, a known target of IFN-γ activity (Fig. 3D). Although MHC class I is also a target of IFN-γ, our IFN-γ gene set was more weakly correlated with tumor MHC class I protein expression than the other tissue biomarkers (pairwise τ = 0.19, $P = 0.02$; Fig. 3D). Together, these data support the notion that baseline IFN-γ and markers of IFN-γ–mediated inflammation, including melanoma-specific MHC class II and PD-L1 expression, are associated with subsequent response to NIVO but not to IPI.

Transcriptional signatures of innate immune cells and response in CheckMate 064

The top 25 immune transcripts associated with a lack of disease progression among patients initially treated with NIVO included transcripts expressed by NK cells (*KLRD1* and *TIGIT*) and those that stimulate NK cells (*IL15*, also important for memory CD8$^+$ T cells). These data suggested that other baseline effector immune cell populations such as NK cells or γδ T cells may be responsible, in part, for IFN-γ and for response after NIVO among patients with loss of melanoma MHC class I expression. To examine this possibility, we manually selected a set of lineage-specific gene transcripts to comprise an NK cell gene set and a γδ T cell gene set, respectively (table S5). Among patients initially treated with NIVO and who achieved a best overall response of complete response, partial response, or stable disease, we observed a significantly higher baseline transcrip-

tional signature of γδ T cells, NK cells, and interleukin 15 (IL-15) compared with those with a best overall response of progressive disease ($P = 0.002$, $P = 0.01$, and $P < 0.001$, respectively, Wilcoxon rank sum test; Fig. 4). This association was not observed among patients initially treated with IPI. The associations between best overall response and the γδ T cell and IL-15 signatures were also significant for patients initially treated with NIVO and with ≤50% tumor MHC class I expression ($P = 0.013$ and $P = 0.0012$, respectively, Wilcoxon rank sum test; Fig. 4). IHC for T cell receptor δ (TCRδ) and CD56 confirmed the presence of γδ T cells and NK cells, respectively, within the tumor microenvironment, including cases with low tumor MHC class I expression (Fig. 4).

DISCUSSION

Combination therapy with NIVO and IPI is known to result in superior overall survival among patients with advanced-stage melanoma compared with either treatment alone (1, 2). These results are consistent with preclinical studies reporting that anti–CTLA-4 and anti–PD-1 treatment promote T cell immunity through distinct and complementary mechanisms. However, T cells must nonetheless recognize tumor cell antigens in the context of MHC to stimulate an antitumor immune response.

We found that the loss of most or all MHC class I protein expression is very common in melanoma before immunotherapy, occurring in 43% of all cases. Attenuated MHC class I protein expression was accompanied by a coordinate reduction in β2M protein and *HLA-A*, *HLA-B*, *HLA-C*, and *B2M* transcripts. However, we could not attribute reduced expression of these genes to disruptive somatic mutations. Whether dysregulation of the MHC class I "master regulator" such as NLRC5 or, potentially, epigenetic silencing of MHC class I–associated genes underlies diminished MHC class I/β2M expression is under investigation (27–29). Regardless of the mechanism, reduction and loss of MHC class I protein expression are common among melanomas before immune checkpoint therapy.

Critically, reduced melanoma MHC class I expression was associated with primary resistance to IPI, but not to NIVO. This

Fig. 3. Predictive value of defined gene set scores derived using RNA-seq data from baseline biopsy samples from CheckMate 064. (**A**) Gene set scores and response at week 13 for patients treated with NIVO (left) or IPI (right). (**B**) Gene set scores and response for the IPI→NIVO arm (left) and NIVO→IPI arm (right). (A) and (B) include gene set scores derived from a published IFN-γ signature (left box plots) (23), the top 25 differentially expressed gene transcripts for distinguishing patients according to best overall response in the NIVO→IPI arm of CheckMate 064 (middle box plots), and a curated set of 13 IFN-γ–related genes derived from the 25-gene set (right box plots). Response is divided according to progressive disease (PD) (red) or nonprogressive disease [complete response (CR), partial response (PR), or stable disease (SD); blue]. Statistical comparisons are based on one-sided Wilcoxon rank sum tests. (**C**) A heat map shows the relative expression of the top 25 gene transcripts differentially expressed between patients with progressive disease from those without progressive disease as best overall response (BOR) using RNA-seq data from baseline biopsy samples in the NIVO→IPI arm ($P = 0.0002$ to 0.01; false discovery rates, 0.14 to 0.27). Each column represents a sample. Rows represent response at week 13 (RESW13I, row 1), best overall response (BORI, row 2), and the top 25 differentially expressed transcripts grouped according to unsupervised hierarchical clustering and color-coded to indicate their relative abundance (rows 3 to 27). Gene transcripts encoding IFN-γ, markers of cells responsible for IFN-γ, transcription factors that promote IFN-γ production, or targets expressed in response to IFN-γ signaling are indicated in blue and comprise the 13 IFN-γ–related gene set. (**D**) Pairwise correlations using Kendall's τ between indicated protein and transcriptional signature biomarkers across all baseline biopsy samples with available data. The empirically derived IFN-γ gene set score positively correlates with baseline melanoma MHC class II protein expression across all samples (Kendall's pairwise correlation $\tau = 0.43$, $P < 0.001$). The IFN-γ gene set score and the previously published IFN-γ signature, respectively, positively correlate with the number of tumor-associated CD3+ ($P < 0.0001$ and $P < 0.0001$), CD4+ ($P = 0.0012$ and $P = 0.0005$), and CD8+ ($P < 0.0001$ and $P < 0.0001$) T cells and with melanoma PD-L1 expression ($P < 0.0001$ and $P < 0.0001$). MHC class I protein expression more weakly positively correlates with our IFN-γ gene set (pairwise $\tau = 0.19$, $P = 0.02$). N.S., not significant; #, number.
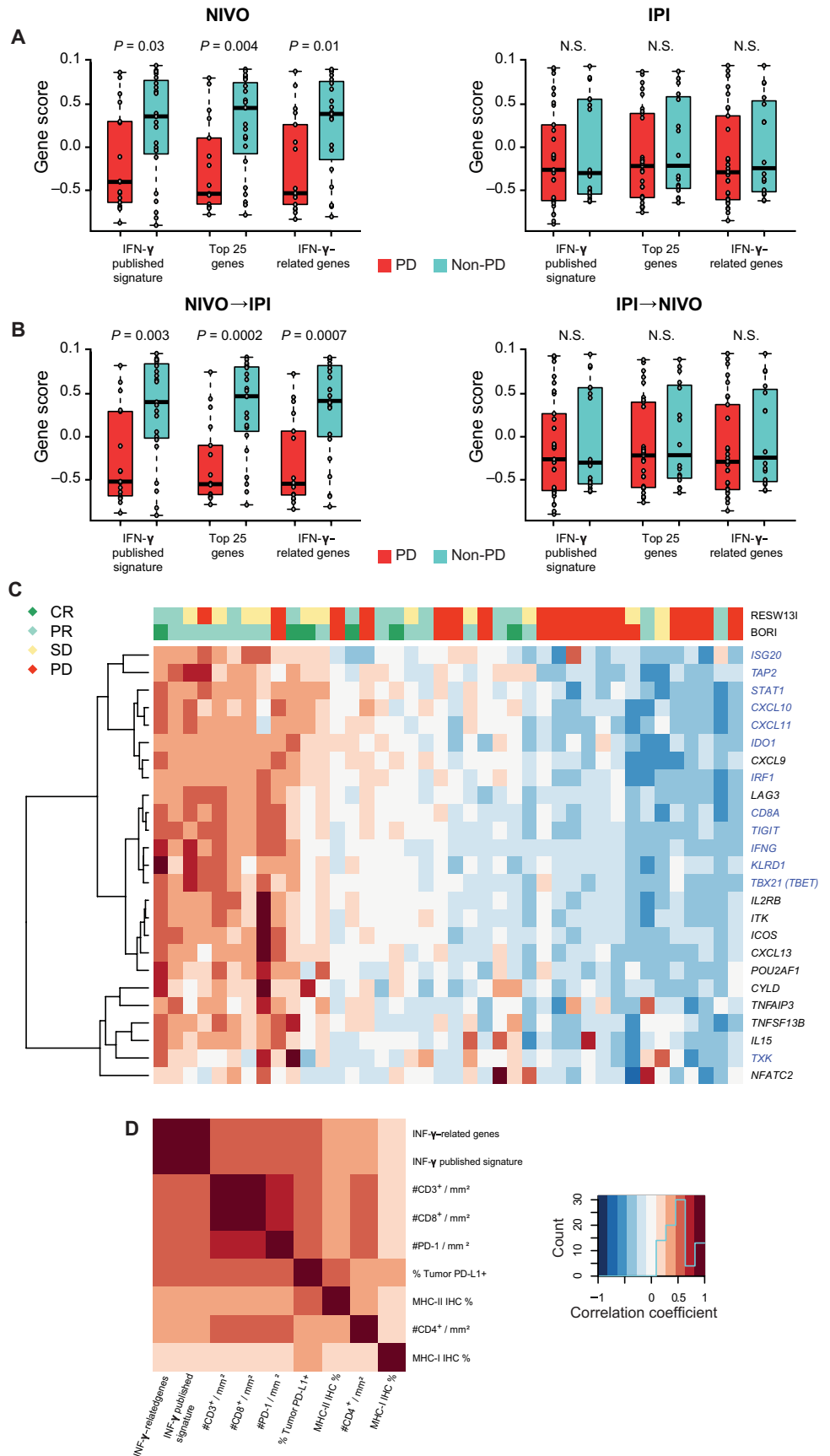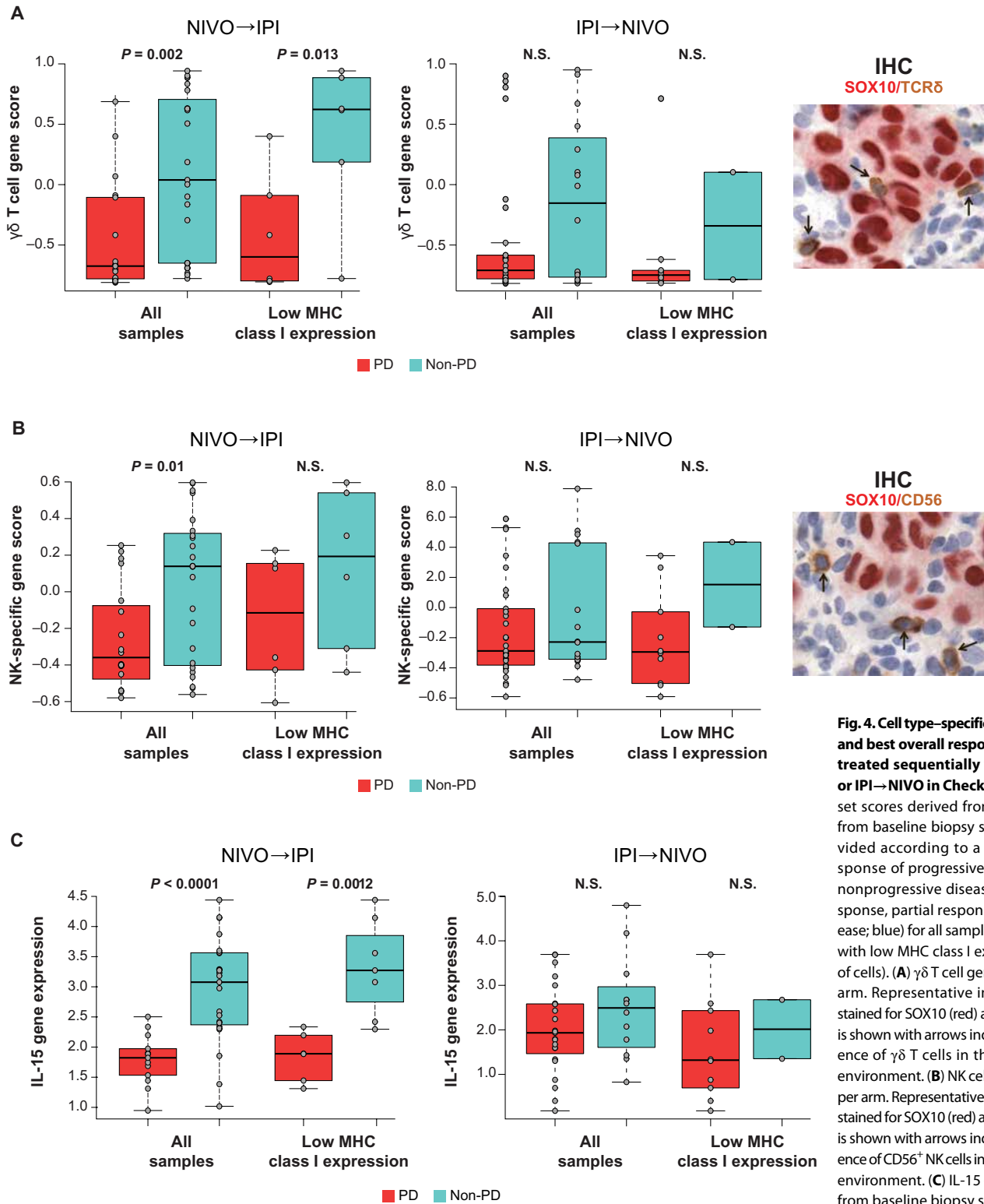
Fig. 4. Cell type–specific gene set scores and best overall response for patients treated sequentially with NIVO→IPI or IPI→NIVO in CheckMate 064. Gene set scores derived from RNA-seq data from baseline biopsy samples were divided according to a best overall response of progressive disease (red) or nonprogressive disease (complete response, partial response, or stable disease; blue) for all samples or for samples with low MHC class I expression (≤50% of cells). (A) γδ T cell gene set scores per arm. Representative image of sample stained for SOX10 (red) and TCRδ (brown) is shown with arrows indicating the presence of γδ T cells in the tumor microenvironment. (B) NK cell gene set scores per arm. Representative image of sample stained for SOX10 (red) and CD56 (brown) is shown with arrows indicating the presence of CD56+ NK cells in the tumor microenvironment. (C) IL-15 gene expression from baseline biopsy samples per arm. Statistical comparisons are based on one-sided Wilcoxon rank sum tests.

association was observed for patients receiving single-agent IPI, was not altered with subsequent switch to NIVO in CheckMate 064, and was validated for patients receiving single-agent IPI until

disease progression in CheckMate 069. More specifically, the loss of MHC class I was highly associated with progressive disease and predicted a lack of clinical response (progressive disease or stable

disease; negative predictive value, 100%) for patients receiving single-agent IPI in CheckMate 069. The HR for survival in the IPI arm of CheckMate 069 (HR = 0.34) was similar to that of the IPI→NIVO arm of CheckMate 064 (HR = 0.38) despite a smaller sample size. Although loss of MHC class I was associated with progressive disease among patients receiving IPI before NIVO, we observed no such association among patients receiving concurrent NIVO and IPI. Thus, in the absence of robust MHC class I antigen presentation, treatment with NIVO early in the course of therapy appears critical.

These observations refine our understanding of anti–CTLA-4 clinical activity (5, 30, 31). Anti–CTLA-4 allows the costimulatory receptor CD28 on T cells to engage CD80/CD86 on APCs laden with tumor antigens and promotes T cell activation during the priming phase of the adaptive immune response in secondary lymphoid organs. In addition, there is increasing evidence that anti–CTLA-4 depletes CTLA-4–expressing T-regulatory cells to increase the relative number of T effector cells at the tumor site (32). Despite the multiple roles of CTLA-4 in regulating the immune response, our data suggest that the major consequence of anti–CTLA-4 therapy is the development of active CD8^{+} effector T cells that require intact MHC class I–mediated antigen presentation by tumor cells to affect tumoricidal activity. The high prevalence of reduced MHC class I expression on melanoma may explain why most patients do not respond to single-agent IPI (33).

We did not find attenuated MHC class I expression to be associated with primary resistance to single-agent NIVO. This result may seem inconsistent with a recent report of an inactivating mutation in *B2M* found in a biopsy sample of recurrent melanoma from a patient with acquired resistance to the anti–PD-1 agent pembrolizumab (22). The reasons for this discrepancy are unclear. First, it is possible that MHC class I expression on a minority of malignant cells is necessary and sufficient for primary response to anti–PD-1 treatment, which can stimulate both innate and adaptive immunity via IFN-γ, but not for primary response to anti–CTLA-4 treatment, which requires high expression of MHC class I to be effective. Second, reduced expression of MHC class I protein reflects general transcriptional repression of multiple genes involved in MHC class I antigen presentation pathway in treatment-naïve melanoma that might be, in part, reversible under the appropriate physiological conditions. Third, it is possible that the MHC dependencies that we observed with initial therapy may change on chronic exposure to immune checkpoint blockade and the eventual emergence of resistance (34). Tumors with acquired resistance to immunotherapy can acquire genetic deficiencies that result in the loss of either constitutive or induced MHC class I (35, 36).

We found that melanoma MHC class II expression was associated with better outcome among patients initially treated with NIVO in CheckMate 064. A switch in therapy to IPI for 13 weeks (followed by maintenance NIVO) did not alter this positive association. This result is both consistent with and validates a previous report that found that focal melanoma MHC class II expression was associated with better outcomes among patients treated with anti–PD-1 or anti–PD-L1 therapy (37).

Tumor antigen presentation via MHC class II may activate tumor-infiltrating CD4^{+} T cells that have T helper or cytotoxic activities and therefore provide an alternative means to promote an adaptive immune response when MHC class I expression is reduced (38). The most potent stimulus for MHC class II expression is IFN-γ (26).

Patients achieving a best overall response of complete response, partial response, or stable disease showed higher expression of *IFNG* and IFN-γ target gene transcripts compared with patients achieving a best overall of progressive disease when initially treated with NIVO. In contrast, neither a previously published and validated IFN-γ signature, predictive of response to pembrolizumab (23), nor our independently derived IFN-γ gene set predicted a lack of disease progression among patients initially treated with IPI. Although IFN-γ promotes MHC class I expression in most cell types, we observed a weaker correlation between the IFN-γ signature and melanoma-specific MHC class I than between the IFN-γ signature and melanoma-specific MHC class II. These results suggest that the MHC protein classes may be differentially regulated on melanoma cells, at least in part.

CD4^{+} T cells and NK cells are primary producers of IFN-γ (26). Thus, CD4^{+} T cells activated via recognition of tumor antigen in the context of MHC class II will produce IFN-γ, which, in turn, will induce additional MHC class II expression on tumor and immune cells at the tumor site. With reduced or absent melanoma MHC class I expression, MHC class II–regulated effector CD4^{+} T cells may have a more important role in tumoricidal function (38, 39). NK cells and γδ T cells are additional non–MHC class I–restricted sources for IFN-γ. Consistent with a role for these innate immune cells in mediating response, we find that patients with higher baseline expression of NK-cell and γδ T cell–associated gene transcripts have better outcomes after treatment with NIVO. However, in general, we observed fewer numbers of CD56^{+} NK cells and TCRδ^{+} T cells than CD3^{+} T cells within the tumor microenvironment. These data suggest that NIVO exerts its effects through several complementary IFN-γ–related innate and adaptive immune pathways when tumor MHC class I is compromised. We did not observe such an association among patients initially treated with IPI.

Despite our findings, there are limitations inherent to our study that will benefit from the analysis of other clinically annotated cohorts by the current and additional methods. Specifically, it will be important to confirm the associations we have observed between tumor-specific MHC class I and II expression and clinical responses to single-agent IPI and NIVO, respectively, in clinical cohorts that include greater patient numbers and with longer clinical follow-up. A further limitation is our reliance upon retrospective analyses. Ideally, our findings will be further validated in trials in which treatment options are determined in accordance with results of tissue-based biomarker studies (that is, MHC class I and II expression and IFN-γ gene set score), as has been done with tumor-specific PD-L1 expression in lung cancer (40). Finally, our IHC analyses are based on manual scoring by trained pathologists. It will be of interest to determine whether more automated methods of marker quantitation can be developed and implemented for routine use. These may include image analysis algorithms trained on the clinically relevant data sets stained for the MHC proteins or quantitative, targeted transcriptional profiling amenable to formalin-fixed paraffin-embedded (FFPE) tissue.

Together, our data provide insights into the baseline biological determinants of clinical response to single-agent and combination anti–CTLA-4 and anti–PD-1 treatment and, by extension, the immune responses augmented by individual and combined therapies. Clinical efficacy of anti–CTLA-4 therapy is dependent on pre-existing, robust expression of MHC class I by tumor cells and is restricted to stimulating an MHC class I–directed cytotoxic T cell immune response. In contrast, efficacy of anti–PD-1 therapy is dependent on at least low-level, preexisting, IFN-γ–mediated inflammation

within the tumor microenvironment and is associated with both adaptive and innate immune responses. Combined immune checkpoint blockade provides a further immune stimulus over individual therapies alone and, in addition, overcomes the limitations of each. Patients treated with the combination of NIVO and IPI did not show dependence on MHC class I expression for clinical response in the CheckMate 069 trial, further supporting the notion that alternative antitumor immune mechanisms are stimulated in patients receiving NIVO, either as a single agent or as part of combination therapy. These data provide a basis to further improve our understanding of the effects of immune checkpoint blockade on effector cells beyond CD8^{+} T cells and suggest future avenues of investigation for manipulating the immune system to effectively treat cancer.

MATERIALS AND METHODS

Study design
The current study used data from two previously published clinical trials. CheckMate 064 was a randomized, open-label, phase 2 study (NCT01783938) evaluating NIVO→IPI versus the reverse treatment sequence IPI→NIVO in patients with histologically confirmed unresectable stage III or stage IV melanoma (fig. S3) (41). Patients were randomized (1:1) without bias either into an induction regimen where NIVO was given at 3 mg/kg every 2 weeks for up to six doses, followed by IPI at 3 mg/kg every 3 weeks for up to four doses, or into a second regimen arm where IPI was followed by NIVO (same dosages). Both cohort arms received NIVO maintenance at 3 mg/kg every 2 weeks until progression, unacceptable toxicity, or for a duration of 2 years from first study treatment. Patient inclusion was limited to treatment-naïve patients or those with one failed nonimmunotherapy systemic treatment, Eastern Cooperative Oncology Group performance status of 0 or 1, and patients with available baseline biopsy tissue. The primary end point of CheckMate 064 was the rate of treatment-related grade 3 to 5 adverse events during the induction period. The secondary end points were response rate as determined by RECIST 1.1 at week 25 and progression rates at weeks 13 and 25. Overall survival analysis was an exploratory end point planned after 65% of the subjects died or 2 years of follow-up time from last subject randomized, whichever came first. The sample size of 138 was not based on power considerations but was chosen to achieve a sufficient level of precision for estimating adverse event rates and provide adequate samples of tumor tissue to achieve stable estimates for exploratory biomarker analyses. All IHC results from patients with evaluable baseline biopsies have been reported; no outliers have been omitted. The schema for CheckMate069 is presented in fig. S3. Its design, including patient selection, randomization, and study end points, closely resembled CheckMate 064 (1). In CheckMate 069, patients receiving IPI alone had the option of receiving NIVO at disease progression (1). Biopsy samples (FFPE and fresh-frozen tissues in CheckMate 064 and FFPE tissues in CheckMate 069) were obtained with approval from institutional review boards.

Chromogenic IHC
Dual IHC for MHC class I (HLA-A, HLA-B, and HLA-C, clone EMR8-5, 1:6000; Abcam) or MHC class II (HLA-DP, HLA-DQ, HLA-DR, clone CR3/43, 1:750; Dako) with the melanoma marker SOX10 (EP268, 1:1500; Cell Marque) was performed using an automated staining system (Bond-III; Leica Biosystems), as previously described (42).

IHC for CD3 (LN10; Leica), CD4 (4B12; Dako), CD8 (C8/144B; Dako), PD-1 (NAT105; Abcam), CD56 (clone 123C3; Dako), TCRδ (clone H-41; Santa Cruz Biotechnology), and β2M (A0072, 1:6000; Dako) was performed either manually (CD3, CD4, CD8, and PD-1) or on Bond RX (β2M, CD56, and TCRδ) per standard protocols. IHC for PD-L1 (28-8; Dako) was performed as part of an investigational use–only kit (PD-L1 IHC pharmDx) on Dako Link 48 (2).

IHC evaluation and scoring
MHC class I, MHC class II, and β2M staining was scored in for the percentage of malignant cells in 10% increments (0 to 100%) with positive membrane staining within the entire tissue section, as determined by the consensus of two pathologists, as previously reported (42). Malignant cells were defined by nuclear staining for the melanoma marker SOX10 and were only scored if they were nucleated and viable. Necrotic or fibrotic tissue was excluded from the analysis. Any MHCI/MHCII/β2M expression in nonmalignant (SOX10-negative) inflammatory cells served as an internal positive staining control. CD3, CD4, CD8, and PD-1 staining was evaluated by pathologist-assisted image analysis (Aperio; Leica Biosystems) (2).

RNA-seq and whole-exome sequencing
RNA and DNA were coextracted by Asuragen Inc. using Qiagen AllPrep DNA/RNA Mini Kits (catalog #80204; Qiagen). RNA-seq was performed by Q2 Solutions/EA Genomics with a minimum of 250 ng of total RNA input using the TruSeq Stranded mRNA with 50 million paired-end reads on Illumina HiSeq. Tumor and normal matched DNA samples were processed for whole-exome sequencing with one normal and two tumor libraries, each using 500 ng of DNA input and constructed with individual barcoded adapters. The libraries were combined into an exome-capture sequencing library using the Roche NimbleGen EZ Exome version 3.0 reagent (Roche Sequencing) following the manufacturer's instructions. Exome sequence data were generated as 2 × 100 base-pair reads on an Illumina HiSeq 2000 instrument (Illumina).

Somatic mutations in the indicated genes were called with MuTect and Strelka algorithms by comparing tumor exome sequencing data with matched normal peripheral blood mononuclear blood samples (43, 44). Mutations were pooled together, annotated with SnpEff software, and further filtered by qualities and matching to known germline polymorphisms from public databases (45). The GATK-CNV best practices pipeline was used to derive deep copy number losses and high copy number gains based on the paired exome sequencing data (46, 47). Gene transcript expression, derived from RNA-seq data, was examined in the space of a curated set of 770 immune-related gene products (48, 49).

Statistical analysis
For clinical response analysis, only patients with complete IHC data (MHC class I, MHC class II, and β2M) were included. Dichotomous cut points for IHC markers were determined to maximize the associations between biomarker high versus low and clinical outcomes (13-week disease progression and overall survival) and were based on 92 patients from CheckMate 064 (IPI→NIVO, n = 42; NIVO→IPI, n = 50) who had complete IHC data. Cut points for 13-week response were estimated using jackknife resampling of receiver operating characteristic curves and Youden's index (50). The optimal threshold for distinguishing patients developing disease progression from those without at week 13 was 30% for

MHC class I with single-agent IPI (there was no threshold for MHC class I expression that reached statistical significance among patients treated with single-agent NIVO) and 1% for MHC class II among patients treated with single-agent NIVO (there was no threshold that reached significance for MHC class II expression among patients treated with single-agent IPI). Cut points for overall survival were estimated using leave-one-out jackknife resampling of the algorithm of Contal-O'Quigley. These were 50% for MHC class I (which was the optimal threshold predicting overall survival among patients initially treated with IPI) and 1% for MHC class II (which was the optimal threshold predicting overall survival among patients initially treated with NIVO). There was no threshold for MHC class I expression and no threshold for MHC class II expression that reached statistical significance for predicting overall survival among patients initially treated with NIVO and IPI, respectively. Only those optimized thresholds for predicting overall survival that reached statistical significance in CheckMate 064 (50%; 1%) were tested for their ability to predict survival and response in CheckMate 069. Cox proportional hazards regression analyses were used to estimate P values and HRs (biomarker high versus low) with 95% Wald CIs. Rates of response and proportions of patients with progressive disease were compared for biomarker high versus low using Fisher's exact tests. Kendall's τ was used to show pairwise correlation between biomarkers for the correlation heat map. Additional details on the methods described above are included in the Supplementary Materials.

SUPPLEMENTARY MATERIALS

www.sciencetranslationalmedicine.org/cgi/content/full/10/450/eaar3342/DC1
Materials and Methods
Fig. S1. Representative IHC images.
Fig. S2. Correlations of MHC class I IHC scores with β2M IHC scores and HLA transcripts.
Fig. S3. Study schemas for the CheckMate 064 and CheckMate 069 trials.
Fig. S4. Comparison of MHC class I and MHC class II expression in paired baseline and week 13 biopsy samples from CheckMate 064.
Table S1. CheckMate 064 MHC class I and MHC class II IHC.
Table S2. Best overall response of PD and non-PD according to optimally defined biomarker thresholds.
Table S3. CheckMate 069 MHC class I and MHC class II IHC.
Table S4. Genes used in the published IFN-γ signature.
Table S5. Genes used in the NK cell and γδ T cell gene sets.
References (51–59)

REFERENCES AND NOTES

1. M. A. Postow, J. Chesney, A. C. Pavlick, C. Robert, K. Grossmann, D. McDermott, G. P. Linette, N. Meyer, J. K. Giguere, S. S. Agarwala, M. Shaheen, M. S. Ernstoff, D. Minor, A. K. Salama, M. Taylor, P. A. Ott, L. M. Rollin, C. Horak, P. Gagnier, J. D. Wolchok, F. S. Hodi, Nivolumab and ipilimumab versus ipilimumab in untreated melanoma. *N. Engl. J. Med.* **372**, 2006–2017 (2015).

2. J. Larkin, V. Chiarion-Sileni, R. Gonzalez, J. J. Grob, C. L. Cowey, C. D. Lao, D. Schadendorf, R. Dummer, M. Smylie, P. Rutkowski, P. F. Ferrucci, A. Hill, J. Wagstaff, M. S. Carlino, J. B. Haanen, M. Maio, I. Marquez-Rodas, G. A. McArthur, P. A. Ascierto, G. V. Long, M. K. Callahan, M. A. Postow, K. Grossmann, M. Sznol, B. Dreno, L. Bastholt, A. Yang, L. M. Rollin, C. Horak, F. S. Hodi, J. D. Wolchok, Combined nivolumab and ipilimumab or monotherapy in untreated melanoma. *N. Engl. J. Med.* **373**, 23–34 (2015).

3. K. S. Peggs, S. A. Quezada, C. A. Chambers, A. J. Korman, J. P. Allison, Blockade of CTLA-4 on both effector and regulatory T cell compartments contributes to the antitumor activity of anti-CTLA-4 antibodies. *J. Exp. Med.* **206**, 1717–1725 (2009).

4. J. D. Wolchok, Y. Saenger, The mechanism of anti-CTLA-4 activity and the negative regulation of T-cell activation. *Oncologist* **13** (suppl. 4), 2–9 (2008).

5. R. J. Greenwald, G. J. Freeman, A. H. Sharpe, The B7 family revisited. *Annu. Rev. Immunol.* **23**, 515–548 (2005).

6. K. E. Pauken, E. J. Wherry, Overcoming T cell exhaustion in infection and cancer. *Trends Immunol.* **36**, 265–276 (2015).

7. S. Spranger, H. K. Koblish, B. Horton, P. A. Scherle, R. Newton, T. F. Gajewski, Mechanism of tumor rejection with doublets of CTLA-4, PD-1/PD-L1, or IDO blockade involves restored IL-2 production and proliferation of CD8+ T cells directly within the tumor microenvironment. *J. Immunother. Cancer* **2**, 3 (2014).

8. J. Duraiswamy, K. M. Kaluza, G. J. Freeman, G. Coukos, Dual blockade of PD-1 and CTLA-4 combined with tumor vaccine effectively restores T-cell rejection function in tumors. *Cancer Res.* **73**, 3591–3603 (2013).

9. S. C. Wei, J. H. Levine, A. P. Cogdill, Y. Zhao, N. A. S. Anang, M. C. Andrews, P. Sharma, J. Wang, J. A. Wargo, D. Pe'er, J. P. Allison, Distinct cellular mechanisms underlie anti-CTLA-4 and anti-PD-1 checkpoint blockade. *Cell* **170**, 1120–1133.e17 (2017).

10. M. M. Gubin, X. Zhang, H. Schuster, E. Caron, J. P. Ward, T. Noguchi, Y. Ivanova, J. Hundal, C. D. Arthur, W.-J. Krebber, G. E. Mulder, M. Toebes, M. D. Vesely, S. S. K. Lam, A. J. Korman, J. P. Allison, G. J. Freeman, A. H. Sharpe, E. L. Pearce, T. N. Schumacher, R. Aebersold, H.-G. Rammensee, C. J. M. Melief, E. R. Mardis, W. E. Gillanders, M. N. Artyomov, R. D. Schreiber, Checkpoint blockade cancer immunotherapy targets tumour-specific mutant antigens. *Nature* **515**, 577–581 (2014).

11. B. Engels, V. H. Engelhard, J. Sidney, A. Sette, D. C. Binder, R. B. Liu, D. M. Kranz, S. C. Meredith, D. A. Rowley, H. Schreiber, Relapse or eradication of cancer is predicted by peptide–major histocompatibility complex affinity. *Cancer Cell* **23**, 516–526 (2013).

12. H. Schreiber, T. H. Wu, J. Nachman, W. M. Kast, Immunodominance and tumor escape. *Semin. Cancer Biol.* **12**, 25–31 (2002).

13. P. C. Tumeh, C. L. Harview, J. H. Yearley, I. P. Shintaku, E. J. M. Taylor, L. Robert, B. Chmielowski, M. Spasic, G. Henry, V. Ciobanu, A. N. West, M. Carmona, C. Kivork, E. Seja, G. Cherry, A. J. Gutierrez, T. R. Grogan, C. Mateus, G. Tomasic, J. A. Glaspy, R. O. Emerson, H. Robins, R. H. Pierce, D. A. Elashoff, C. Robert, A. Ribas, PD-1 blockade induces responses by inhibiting adaptive immune resistance. *Nature* **515**, 568–571 (2014).

14. R. S. Herbst, J.-C. Soria, M. Kowanetz, G. D. Fine, O. Hamid, M. S. Gordon, J. A. Sosman, D. F. McDermott, J. D. Powderly, S. N. Gettinger, H. E. K. Kohrt, L. Horn, D. P. Lawrence, S. Rost, M. Leabman, Y. Xiao, A. Mokatrin, H. Koeppen, P. S. Hegde, I. Mellman, D. S. Chen, F. S. Hodi, Predictive correlates of response to the anti-PD-L1 antibody MPDL3280A in cancer patients. *Nature* **515**, 563–567 (2014).

15. Z. A. Cooper, A. Reuben, C. N. Spencer, P. A. Prieto, J. L. Austin-Breneman, H. Jiang, C. Haymaker, V. Gopalakrishnan, M. T. Tetzlaff, D. T. Frederick, R. J. Sullivan, R. N. Amaria, S. P. Patel, P. Hwu, S. E. Woodman, I. C. Glitza, A. Diab, L. M. Vence, J. Rodriguez-Canales, E. R. Parra, I. I. Wistuba, L. M. Coussens, A. H. Sharpe, K. T. Flaherty, J. E. Gershenwald, L. Chin, M. A. Davies, K. Clise-Dwyer, J. P. Allison, P. Sharma, J. A. Wargo, Distinct clinical patterns and immune infiltrates are observed at time of progression on targeted therapy versus immune checkpoint blockade for melanoma. *Oncoimmunology* **5**, e1136044 (2016).

16. P.-L. Chen, W. Roh, A. Reuben, Z. A. Cooper, C. N. Spencer, P. A. Prieto, J. P. Miller, R. L. Bassett, V. Gopalakrishnan, K. Wani, M. P. De Macedo, J. L. Austin-Breneman, H. Jiang, Q. Chang, S. M. Reddy, W.-S. Chen, M. T. Tetzlaff, R. J. Broaddus, M. A. Davies, J. E. Gershenwald, L. Haydu, A. J. Lazar, S. P. Patel, P. Hwu, W.-J. Hwu, A. Diab, I. C. Glitza, S. E. Woodman, L. M. Vence, I. I. Wistuba, R. N. Amaria, L. N. Kwong, V. Prieto, R. E. Davis, W. Ma, W. W. Overwijk, A. H. Sharpe, J. Hu, P. A. Futreal, J. Blando, P. Sharma, J. P. Allison, L. Chin, J. A. Wargo, Analysis of immune signatures in longitudinal tumor samples yields insight into biomarkers of response and mechanisms of resistance to immune checkpoint blockade. *Cancer Discov.* **6**, 827–837 (2016).

17. A. I. Daud, J. D. Wolchok, C. Robert, W.-J. Hwu, J. S. Weber, A. Ribas, F. S. Hodi, A. M. Joshua, R. Kefford, P. Hersey, R. Joseph, T. C. Gangadhar, R. Dronca, A. Patnaik, H. Zarour, C. Roach, G. Toland, J. K. Lunceford, X. N. Li, K. Emancipator, M. Dolled-Filhart, S. P. Kang, S. Ebbinghaus, O. Hamid, Programmed death-ligand 1 expression and response to the anti-programmed death 1 antibody pembrolizumab in melanoma. *J. Clin. Oncol.* **34**, 4102–4109 (2016).

18. R. E. Vilain, A. M. Menzies, J. S. Wilmott, H. Kakavand, J. Madore, A. Guminski, E. Liniker, B. Y. Kong, A. J. Cooper, J. R. Howle, R. P. M. Saw, V. Jakrot, S. Lo, J. F. Thompson, M. S. Carlino, R. F. Kefford, G. V. Long, R. A. Scolyer, Dynamic changes in PD-L1 expression and immune infiltrates early during treatment predict response to PD-1 blockade in melanoma. *Clin. Cancer Res.* **23**, 5024–5033 (2017).

19. A. Snyder, V. Makarov, T. Merghoub, J. Yuan, J. M. Zaretsky, A. Desrichard, L. A. Walsh, M. A. Postow, P. Wong, T. S. Ho, T. J. Hollmann, C. Bruggeman, K. Kannan, Y. Li, C. Elipenahli, C. Liu, C. T. Harbison, L. Wang, A. Ribas, J. D. Wolchok, T. A. Chan, Genetic basis for clinical response to CTLA-4 blockade in melanoma. *N. Engl. J. Med.* **371**, 2189–2199 (2014).

20. E. M. Van Allen, D. Miao, B. Schilling, S. A. Shukla, C. Blank, L. Zimmer, A. Sucker, U. Hillen, M. H. G. Foppen, S. M. Goldinger, J. Utikal, J. C. Hassel, B. Weide, K. C. Kaehler, C. Loquai, P. Mohr, R. Gutzmer, R. Dummer, S. Gabriel, C. J. Wu, D. Schadendorf, L. A. Garraway, Genomic correlates of response to CTLA-4 blockade in metastatic melanoma. *Science* **350**, 207–211 (2015).

21. N. A. Rizvi, M. D. Hellmann, A. Snyder, P. Kvistborg, V. Makarov, J. J. Havel, W. Lee, J. Yuan, P. Wong, T. S. Ho, M. L. Miller, N. Rekhtman, A. L. Moreira, F. Ibrahim, C. Bruggeman,

B. Gasmi, R. Zappasodi, Y. Maeda, C. Sander, E. B. Garon, T. Merghoub, J. D. Wolchok, T. N. Schumacher, T. A. Chan, Mutational landscape determines sensitivity to PD-1 blockade in non–small cell lung cancer. *Science* **348**, 124–128 (2015).

22. J. M. Zaretsky, A. Garcia-Diaz, D. S. Shin, H. Escuin-Ordinas, W. Hugo, S. Hu-Lieskovan, D. Y. Torrejon, G. Abril-Rodriguez, S. Sandoval, L. Barthly, J. Saco, B. H. Moreno, R. Mezzadra, B. Chmielowski, K. Ruchalski, I. P. Shintaku, P. J. Sanchez, C. Puig-Saus, G. Cherry, E. Seja, X. Kong, J. Pang, B. Berent-Maoz, B. Comin-Anduix, T. G. Graeber, P. C. Tumeh, T. N. M. Schumacher, R. S. Lo, A. Ribas, Mutations associated with acquired resistance to PD-1 blockade in melanoma. *N. Engl. J. Med.* **375**, 819–829 (2016).

23. M. Ayers, J. Lunceford, M. Nebozhyn, E. Murphy, A. Loboda, D. R. Kaufman, A. Albright, J. D. Cheng, S. P. Kang, V. Shankaran, S. A. Piha-Paul, J. Yearley, T. Y. Seiwert, A. Ribas, T. K. McClanahan, IFN-γ–related mRNA profile predicts clinical response to PD-1 blockade. *J. Clin. Invest.* **127**, 2930–2940 (2017).

24. E. Marcenaro, S. Carlomagno, S. Pesce, M. Della Chiesa, S. Parolini, A. Moretta, S. Sivori, NK cells and their receptors during viral infections. *Immunotherapy* **3**, 1075–1086 (2011).

25. W. C. Dougall, S. Kurtulus, M. J. Smyth, A. C. Anderson, TIGIT and CD96: New checkpoint receptor targets for cancer immunotherapy. *Immunol. Rev.* **276**, 112–120 (2017).

26. M. A. Farrar, R. D. Schreiber, The molecular cell biology of interferon-gamma and its receptor. *Annu. Rev. Immunol.* **11**, 571–611 (1993).

27. S. Yoshihama, J. Roszik, I. Downs, T. B. Meissner, S. Vijayan, B. Chapuy, T. Sidiq, M. A. Shipp, G. A. Lizee, K. S. Kobayashi, NLRC5/MHC class I transactivator is a target for immune evasion in cancer. *Proc. Natl. Acad. Sci. U.S.A.* **113**, 5999–6004 (2016).

28. S. Yoshihama, S. Vijayan, T. Sidiq, K. S. Kobayashi, NLRC5/CITA: A key player in cancer immune surveillance. *Trends Cancer* **3**, 28–38 (2017).

29. K. S. Kobayashi, P. J. van den Elsen, NLRC5: A key regulator of MHC class I-dependent immune responses. *Nat. Rev. Immunol.* **12**, 813–820 (2012).

30. K. S. Peggs, S. A. Quezada, J. P. Allison, Cell intrinsic mechanisms of T-cell inhibition and application to cancer therapy. *Immunol. Rev.* **224**, 141–165 (2008).

31. T. Pentcheva-Hoang, E. Corse, J. P. Allison, Negative regulators of T-cell activation: Potential targets for therapeutic intervention in cancer, autoimmune disease, and persistent infections. *Immunol. Rev.* **229**, 67–87 (2009).

32. T. R. Simpson, F. Li, W. Montalvo-Ortiz, M. A. Sepulveda, K. Bergerhoff, F. Arce, C. Roddie, J. Y. Henry, H. Yagita, J. D. Wolchok, K. S. Peggs, J. V. Ravetch, J. P. Allison, S. A. Quezada, Fc-dependent depletion of tumor-infiltrating regulatory T cells co-defines the efficacy of anti-CTLA-4 therapy against melanoma. *J. Exp. Med.* **210**, 1695–1710 (2013).

33. F. S. Hodi, S. J. O'Day, D. F. McDermott, R. W. Weber, J. A. Sosman, J. B. Haanen, R. Gonzalez, C. Robert, D. Schadendorf, J. C. Hassel, W. Akerley, A. J. M. van den Eertwegh, J. Lutzky, P. Lorigan, J. M. Vaubel, G. P. Linette, D. Hogg, C. H. Ottensmeier, C. Lebbé, C. Peschel, I. Quirt, J. I. Clark, J. D. Wolchok, J. S. Weber, J. Tian, M. J. Yellin, G. M. Nichol, A. Hoos, W. J. Urba, Improved survival with ipilimumab in patients with metastatic melanoma. *N. Engl. J. Med.* **363**, 711–723 (2010).

34. J. L. Benci, B. Xu, Y. Qiu, T. J. Wu, H. Dada, C. Twyman-Saint Victor, D. Cucolo, D. S. M. Lee, K. E. Pauken, A. C. Huang, T. C. Gangadhar, R. K. Amaravadi, L. M. Schuchter, M. D. Feldman, H. Ishwaran, R. H. Vonderheide, A. Maity, E. J. Wherry, A. J. Minn, Tumor interferon signaling regulates a multigenic resistance program to immune checkpoint blockade. *Cell* **167**, 1540–1554.e12 (2016).

35. S. Gettinger, J. Choi, K. Hastings, A. Truini, I. Datar, R. Sowell, A. Wurtz, W. Dong, G. Cai, M. A. Melnick, V. Y. Du, J. Schlessinger, S. B. Goldberg, A. Chiang, M. F. Sanmamed, I. Melero, J. Agorreta, L. M. Montuenga, R. Lifton, S. Ferrone, P. Kavathas, D. L. Rimm, S. M. Kaech, K. Schalper, R. S. Herbst, K. Politi, Impaired HLA class I antigen processing and presentation as a mechanism of acquired resistance to immune checkpoint inhibitors in lung cancer. *Cancer Discov.* **7**, 1420–1435 (2017).

36. J. Gao, L. Z. Shi, H. Zhao, J. Chen, L. Xiong, Q. He, T. Chen, J. Roszik, C. Bernatchez, S. E. Woodman, P.-L. Chen, P. Hwu, J. P. Allison, A. Futreal, J. A. Wargo, P. Sharma, Loss of IFN-γ pathway genes in tumor cells as a mechanism of resistance to anti-CTLA-4 therapy. *Cell* **167**, 397–404.e9 (2016).

37. D. B. Johnson, M. V. Estrada, R. Salgado, V. Sanchez, D. B. Doxie, S. R. Opalenik, A. E. Vilgelm, E. Feld, A. S. Johnson, A. R. Greenplate, M. E. Sanders, C. M. Lovly, D. T. Frederick, M. C. Kelley, A. Richmond, J. M. Irish, Y. Shyr, R. J. Sullivan, I. Puzanov, J. A. Sosman, J. M. Balko, Melanoma-specific MHC-II expression represents a tumour-autonomous phenotype and predicts response to anti-PD-1/PD-L1 therapy. *Nat. Commun.* **7**, 10582 (2016).

38. S. Kitano, T. Tsuji, C. Liu, D. Hirschhorn-Cymerman, C. Kyi, Z. Mu, J. P. Allison, S. Gnjatic, J. D. Yuan, J. D. Wolchok, Enhancement of tumor-reactive cytotoxic CD4+ T cell responses after ipilimumab treatment in four advanced melanoma patients. *Cancer Immunol. Res.* **1**, 235–244 (2013).

39. D. Hirschhorn-Cymerman, S. Budhu, S. Kitano, C. Liu, F. Zhao, H. Zhong, A. M. Lesokhin, F. Avogadri-Connors, J. Yuan, Y. Li, A. N. Houghton, T. Merghoub, J. D. Wolchok, Induction of tumoricidal function in CD4+ T cells is associated with concomitant memory and terminally differentiated phenotype. *J. Exp. Med.* **209**, 2113–2126 (2012).

40. M. Reck, D. Rodríguez-Abreu, A. G. Robinson, R. Hui, T. Csőszi, A. Fülöp, M. Gottfried, N. Peled, A. Tafreshi, S. Cuffe, M. O'Brien, S. Rao, K. Hotta, M. A. Leiby, G. M. Lubiniecki, Y. Shentu, R. Rangwala, J. R. Brahmer; KEYNOTE-024 Investigators, Pembrolizumab versus chemotherapy for PD-L1-positive non-small-cell lung cancer. *N. Engl. J. Med.* **375**, 1823–1833 (2016).

41. J. S. Weber, G. Gibney, R. J. Sullivan, J. A. Sosman, C. L. Slingluff Jr., D. P. Lawrence, T. F. Logan, L. M. Schuchter, S. Nair, L. Fecher, E. I. Buchbinder, E. Berghorn, M. Ruisi, G. Kong, J. Jiang, C. Horak, F. S. Hodi, Sequential administration of nivolumab and ipilimumab with a planned switch in patients with advanced melanoma (CheckMate 064): An open-label, randomised, phase 2 trial. *Lancet Oncol.* **17**, 943–955 (2016).

42. M. G. M. Roemer, R. H. Advani, R. A. Redd, G. S. Pinkus, Y. Natkunam, A. H. Ligon, C. F. Connelly, C. J. Pak, C. D. Carey, S. E. Daadi, B. Chapuy, D. de Jong, R. T. Hoppe, D. S. Neuberg, M. A. Shipp, S. J. Rodig, Classical Hodgkin lymphoma with reduced β2M/MHC class I expression is associated with inferior outcome independent of 9p24.1 status. *Cancer Immunol. Res.* **4**, 910–916 (2016).

43. K. Cibulskis, M. S. Lawrence, S. L. Carter, A. Sivachenko, D. Jaffe, C. Sougnez, S. Gabriel, M. Meyerson, E. S. Lander, G. Getz, Sensitive detection of somatic point mutations in impure and heterogeneous cancer samples. *Nat. Biotechnol.* **31**, 213–219 (2013).

44. C. T. Saunders, W. S. W. Wong, S. Swamy, J. Becq, L. J. Murray, R. K. Cheetham, Strelka: Accurate somatic small-variant calling from sequenced tumor–normal sample pairs. *Bioinformatics* **28**, 1811–1817 (2012).

45. P. Cingolani, A. Platts, L. L. Wang, M. Coon, T. Nguyen, L. Wang, S. J. Land, X. Lu, D. M. Ruden, A program for annotating and predicting the effects of single nucleotide polymorphisms, SnpEff: SNPs in the genome of Drosophila melanogaster strain w1118; iso-2; iso-3. *Fly* **6**, 80–92 (2012).

46. A. McKenna, M. Hanna, E. Banks, A. Sivachenko, K. Cibulskis, A. Kernytsky, K. Garimella, D. Altshuler, S. Gabriel, M. Daly, M. A. DePristo, The Genome Analysis Toolkit: A MapReduce framework for analyzing next-generation DNA sequencing data. *Genome Res.* **20**, 1297–1303 (2010).

47. G. A. Van der Auwera, M. O. Carneiro, C. Hartl, R. Poplin, G. del Angel, A. Levy-Moonshine, T. Jordan, K. Shakir, D. Roazen, J. Thibault, E. Banks, K. V. Garimella, D. Altshuler, S. Gabriel, M. A. DePristo, From FastQ data to high confidence variant calls: The Genome Analysis Toolkit best practices pipeline. *Curr. Protoc. Bioinformatics* **43**, 11.10.1–11.10.33 (2013).

48. S. C. Bresler, L. Min, S. J. Rodig, A. C. Walls, S. Xu, S. Geng, F. S. Hodi, G. F. Murphy, C. G. Lian, Gene expression profiling of anti-CTLA4-treated metastatic melanoma in patients with treatment-induced autoimmunity. *Lab. Invest.* **97**, 207–216 (2017).

49. A. Cesano, nCounter® PanCancer immune profiling panel (NanoString Technologies, Inc., Seattle, WA). *J. Immunother. Cancer* **3**, 42 (2015).

50. W. J. Youden, Index for rating diagnostic tests. *Cancer* **3**, 32–35 (1950).

51. S. Anders, P. T. Pyl, W. Huber, HTSeq—A Python framework to work with high-throughput sequencing data. *Bioinformatics* **31**, 166–169 (2015).

52. M. D. Robinson, D. J. McCarthy, G. K. Smyth, edgeR: A bioconductor package for differential expression analysis of digital gene expression data. *Bioinformatics* **26**, 139–140 (2010).

53. D. J. McCarthy, Y. Chen, G. K. Smyth, Differential expression analysis of multifactor RNA-Seq experiments with respect to biological variation. *Nucleic Acids Res.* **40**, 4288–4297 (2012).

54. M. D. Robinson, A. Oshlack, A scaling normalization method for differential expression analysis of RNA-seq data. *Genome Biol.* **11**, R25 (2010).

55. R. Patro, G. Duggal, M. I. Love, R. A. Irizarry, C. Kingsford, Salmon provides fast and bias-aware quantification of transcript expression. *Nat. Methods* **14**, 417–419 (2017).

56. M. Griffith, O. L. Griffith, S. M. Smith, A. Ramu, M. B. Callaway, A. M. Brummett, M. J. Kiwala, A. C. Coffman, A. A. Regier, B. J. Oberkfell, G. E. Sanderson, T. P. Mooney, N. G. Nutter, E. A. Belter, F. Du, R. L. Long, T. E. Abbott, I. T. Ferguson, D. L. Morton, M. M. Burnett, J. V. Weible, J. B. Peck, A. Dukes, J. F. McMichael, J. T. Lolofie, B. R. Derickson, J. Hundal, Z. L. Skidmore, B. J. Ainscough, N. D. Dees, W. S. Schierding, C. Kandoth, K. H. Kim, C. Lu, C. C. Harris, N. Maher, C. A. Maher, V. J. Magrini, B. S. Abbott, K. Chen, E. Clark, I. Das, X. Fan, A. E. Hawkins, T. G. Hepler, T. N. Wylie, S. M. Leonard, W. E. Schroeder, X. Shi, L. K. Carmichael, M. R. Weil, R. W. Wohlstadter, G. Stiehr, M. D. McLellan, C. S. Pohl, C. A. Miller, D. C. Koboldt, J. R. Walker, J. M. Eldred, D. E. Larson, D. J. Dooling, L. Ding, E. R. Mardis, R. K. Wilson, Genome Modeling System: A knowledge management platform for genomics. *PLOS Comput. Biol.* **11**, e1004274 (2015).

57. H. Li, R. Durbin, Fast and accurate short read alignment with Burrows–Wheeler transform. *Bioinformatics* **25**, 1754–1760 (2009).

58. M. E. Ritchie, B. Phipson, D. Wu, Y. Hu, C. W. Law, W. Shi, G. K. Smyth, *limma* powers differential expression analyses for RNA-sequencing and microarray studies. *Nucleic Acids Res.* **43**, e47 (2015).

59. S. Hänzelmann, R. Castelo, J. Guinney, GSVA: Gene set variation analysis for microarray and RNA-seq data. *BMC Bioinformatics* **14**, 7 (2013).

Citation: S. J. Rodig, D. Gusenleitner, D. G. Jackson, E. Gjini, A. Giobbie-Harder, C. Jin, H. Chang, S. B. Lovitch, C. Horak, J. S. Weber, J. L. Weirather, J. D. Wolchok, M. A. Postow, A. C. Pavlick, J. Chesney, F. S. Hodi, MHC proteins confer differential sensitivity to CTLA-4 and PD-1 blockade in untreated metastatic melanoma. *Sci. Transl. Med.* **10**, eaar3342 (2018).

HIV

Anti-α4β7 therapy targets lymphoid aggregates in the gastrointestinal tract of HIV-1–infected individuals

Mathieu Uzzan[1,2], Minami Tokuyama[3], Adam K. Rosenstein[1,2], Costin Tomescu[4], Ivo N. SahBandar[5], Huaibin M. Ko[2,3], Louise Leyre[6], Anupa Chokola[7], Emma Kaplan-Lewis[8], Gabriela Rodriguez[8], Akihiro Seki[1,2], Michael J. Corley[5], Judith Aberg[8], Annalena La Porte[7,8], Eun-young Park[5], Hideki Ueno[7], Ioannis Oikonomou[9], Itai Doron[10], Iliyan D. Iliev[10], Benjamin K. Chen[1,7,8], Jennifer Lui[1,2], Timothy W. Schacker[11], Glaucia C. Furtado[1], Sergio A. Lira[1], Jean-Frederic Colombel[2], Amir Horowitz[1], Jean K. Lim[8], Nicolas Chomont[6], Adeeb H. Rahman[12,13], Luis J. Montaner[4], Lishomwa C. Ndhlovu[5], Saurabh Mehandru[1,2]*

Gut homing CD4+ T cells expressing the integrin α4β7 are early viral targets and contribute to HIV-1 pathogenesis, likely by seeding the gastrointestinal (GI) tract with HIV. Although simianized anti-α4β7 monoclonal antibodies have shown promise in preventing or attenuating the disease course of simian immunodeficiency virus in nonhuman primate studies, the mechanisms of drug action remain elusive. We present a cohort of individuals with mild inflammatory bowel disease and concomitant HIV-1 infection receiving anti-α4β7 treatment. By sampling the immune inductive and effector sites of the GI tract, we have discovered that anti-α4β7 therapy led to a significant and unexpected attenuation of lymphoid aggregates, most notably in the terminal ileum. Given that lymphoid aggregates serve as important sanctuary sites for maintaining viral reservoirs, their attrition by anti-α4β7 therapy has important implications for HIV-1 therapeutics and eradication efforts and defines a rational basis for the use of anti-α4β7 therapy in HIV-1 infection.

INTRODUCTION

Lentiviruses such as human immunodeficiency virus (HIV) and simian immunodeficiency virus (SIV) are uniquely adapted to infect activated, memory CD4+ T cells that are specifically enriched at mucosal surfaces (1). Consequently, mucosal tissues including those of the gastrointestinal (GI) tract play a critical role in disease pathogenesis during acute (2, 3) and chronic HIV-1 infection (4).

The GI tract can be immunologically subclassified into inductive and effector sites (5). Aggregates of lymphoid tissue, including Peyer's patches (PPs) and isolated lymphoid follicles (intrinsic to the bowel wall) and mesenteric lymph nodes (extrinsic to the bowel wall), serve as the major immune inductive sites. Naïve T and B cells express integrin α4β7 (α4β7), which mediates their migration into the inductive sites through specific interactions with mucosal addressin cell adhesion molecule-1 (MAdCAM-1) (6). Notably, the expression of α4β7 on naïve T and B cells is significantly lower than its expression on memory cells (6). PP-resident dendritic cells (DCs) prime naïve T and B cells and simultaneously induce the expression of α4β7 in a retinoic acid and transforming growth factor–β–dependent fashion (7). These α4β7hi, gut-primed, antigen-experienced memory cells egress into the draining lymph and subsequently into circulation and home to immune effector sites such as intestinal lamina propria, again via specific interactions between MAdCAM-1 and α4β7 (8). Although the putative mechanism of action (MOA) of anti-α4β7 therapy is to prevent the entry of α4β7hi memory T cells into the intestinal lamina propria, to date, the published reports show no change in the frequency of lamina propria CD4+ T cells after anti-α4β7 therapy, either in SIV-infected macaques (9) or in humans with inflammatory bowel disease (IBD) (10). The effects of anti-α4β7 therapy on lymphoid aggregates, where cellular entry is also α4β7-MAdCAM–dependent (6), remain unappreciated.

The pathogenesis of HIV-1 infection intersects with intestinal homing pathways at multiple levels that are yet poorly understood. GI-resident CD4+ T cells are preferentially targeted during acute HIV and SIV. Regardless of the route of infection and mode of virus delivery, intestinal CD4+ T cells are profoundly depleted during the earliest stages of HIV-1 and SIV infection (11). This strongly suggests that HIV-1, either cell-free or cell-associated, has evolved specific mechanisms to localize to GI tract during acute infection to infect CCR5-expressing (12) physiologically activated memory T cells (13, 14) that are exceptionally HIV-1 susceptible (2). In this regard, studies have reported a direct interaction between α4β7 and the viral envelope (15–17). Thus, HIV-1–susceptible α4β7+CD4+ T cells may serve to deliver the virus into the gut tissues.

Multiple lines of evidence demonstrate that α4β7-expressing cells represent early targets for the virus (18–22). This was highlighted in a recent report, demonstrating that preinfection frequencies of α4β7 on circulating CD4+ T cells may predict the risk of HIV-1 acquisition and disease progression independent of other T cell phenotypes and genital inflammation in a large cohort of at-risk South African women

[1]Immunology Institute, Icahn School of Medicine at Mount Sinai, New York, NY 10029, USA. [2]Division of Gastroenterology, Department of Medicine, Icahn School of Medicine at Mount Sinai, New York, NY 10029, USA. [3]Department of Pathology, Icahn School of Medicine at Mount Sinai, New York, NY 10029, USA. [4]Wistar Institute, Philadelphia, PA 19104, USA. [5]Department of Tropical Medicine, John A. Burns School of Medicine, University of Hawaii, Honolulu, HI 96813, USA. [6]Centre de recherche du Centre hospitalier de l'Université de Montréal and Department of Microbiology, Infectiology and Immunology, Université de Montréal, Montréal, Québec H2X 0A9, Canada. [7]Department of Microbiology, Icahn School of Medicine at Mount Sinai, New York, NY 10029, USA. [8]Division of Infectious Disease, Department of Medicine, Icahn School of Medicine at Mount Sinai, New York, NY 10029, USA. [9]Division of Gastroenterology, Rush University, Chicago, IL 60612, USA. [10]Gastroenterology and Hepatology Divison, Department of Medicine, Weill Cornell Medicine, New York, NY 10065, USA. [11]Department of Medicine, Medical School, University of Minnesota, Minneapolis, MN 55455, USA. [12]Human Immune Monitoring Center, Icahn School of Medicine at Mount Sinai, New York, NY 10029, USA. [13]Department of Genetics and Genomic Sciences, Icahn School of Medicine at Mount Sinai, New York, NY 10029, USA.
*Corresponding author. Email: saurabh.mehandru@mssm.edu

(23). Supporting this finding, sexually transmitted diseases that have been linked with increased risk of HIV-1 acquisition increase the frequency of $\alpha4\beta7^+CD4^+$ memory T cells in both the mucosa and blood (24, 25).

Because of the important role of $\alpha4\beta7^+CD4^+$ T cells in viral pathogenesis, anti-$\alpha4\beta7$ therapy has been considered in the management of HIV-1 infection. However, no human studies are available to date. In nonhuman primate (NHP) models, using simianized anti-$\alpha4\beta7$ antibodies has shown promising results. Salient among these studies is the demonstration of disease prevention or an attenuated disease course when anti-$\alpha4\beta7$ antibodies preceded low-dose repeated intravaginal SIV challenge (26). In addition, a recent report found that SIV-infected macaques that were treated during acute infection with combination antiretroviral therapy (cART) and anti-$\alpha4\beta7$ therapy (or isotype control) achieved long-term viremic control after cART and antibody interruption, whereas isotype-treated animals became viremic (27). Despite multiple NHP studies, clear mechanisms underlying the potential efficacy of anti-$\alpha4\beta7$ therapy in HIV (SIV) infection remain elusive.

Although no HIV-related studies have been reported to our knowledge, anti-$\alpha4\beta7$ therapy [vedolizumab (VDZ)] has become a frontline strategy in the management of patients with IBD (28, 29), where it has demonstrated strong efficacy and an excellent safety profile (30). To determine VDZ's role in HIV-1 infection, we have assembled a cohort of IBD patients with concomitant HIV-1 infection. Here, we provide data describing the safety and the immunological and virological effects of anti-$\alpha4\beta7$ therapy in HIV-1–infected patients receiving VDZ therapy over 30 weeks, with detailed analyses in the GI tissue and in peripheral blood.

RESULTS
VDZ was administered safely and without any serious adverse events to patients with HIV-1 infection
Six patients (five males and one female) with a median age of 51.7 years (interquartile range, 36.8 to 62.2) were followed prospectively for 30 weeks after VDZ treatment. Five were receiving cART for a minimum of 5.6 years and had an undetectable plasma viral load at VDZ start (threshold of 20 viral copies/ml). One patient (583-016)

was cART-treated for 9 months and had a plasma viral load of 156 copies/ml at the time of VDZ initiation. In one subject (583-004), colonoscopy could not be performed before treatment due to logistical reasons (the patient had already received the first dose of VDZ as the colonoscopy was being scheduled). Therefore, immunological analyses before and after treatment are being reported on five of six patients. Detailed HIV characteristics are shown in Table 1.

All patients included in the study had very mild IBD activity (table S1), characterized by mild proctitis and endoscopically normal appearing colonic and ileal mucosa with the exception of subject 583-016 where endoscopic inflammation was observed up to 25 cm from the anal verge. However, proximal parts of the colon and the terminal ileum (TI), where study-related biopsies were obtained, were normal in 583-016. None of the study subjects had pancolitis, history of bowel surgery, or previous use of biologic medications, all signifying severe disease (31, 32). In addition, and as further evidence of mild IBD, five of six patients had normal levels of complement-reactive protein (CRP) at the time of starting VDZ (583-016 had a CRP of 16.5 mg/liter at the time of recruitment). Finally, histology, arguably the gold standard for assessment of mucosal inflammation, showed only a mild increase in inflammatory cells limited to the rectum of five of six patients. The TI and left colon (LC), sites where immunological and virological analyses were performed, were histologically normal in each of the study subjects (fig. S1).

Patients were monitored with serial laboratory and clinical assessments. One of the six patients reported mild, self-limited nasopharyngitis, a previously reported adverse effect of VDZ (33). Two of six patients reported mild, self-limited headache, and one patient had intravenous infiltration during infusion. No other adverse events (AEs) or serious AEs related to VDZ were reported during the course of 30 weeks of follow-up, highlighting the safety of this drug in our cohort of HIV-1–infected subjects. These data mirror previous, extensive data in IBD (33).

Anti-$\alpha4\beta7$ therapy results in a significant reduction in B cell subsets within the GI tract
In previous studies in subjects with acute HIV-1 infection, we have observed a profound reduction in CD4$^+$ T cells in the GI lamina propria

Table 1. HIV-related clinical characteristics. F, female; M, male. ATV, atazanavir; COBI, cobicistat; DTG, dolutegravir; EVG, elvitegravir; FPV, fosamprenavir; FTC, emtricitabine; TAF, tenofovir alafenamide; TDF, tenofovir disoproxil fumarate.

ID	Sex	Age at VDZ (years)	CD4 count at VDZ initiation (cells/μl) (%)	HIV viral load* at VDZ initiation (copies/ml)	Duration of HIV infection[†] at VDZ initiation (years)	Duration of ART at VDZ initiation (years)	ART regimen
583-004[‡]	F	64.1	634 (34%)	<20	28.2	>20	DTG FTC TDF
583-012	M	46.8	834 (39%)	<20	14.2	14	DTG FTC TDF
583-013	M	56.6	632 (37%)	<20	21.9	21.8	FPV FTC TDF
583-016	M	24.1	709 (25%)	156	0.9	0.8	EVG COBI FTC TDF
583-017	M	66.7	683 (44%)	<20	28	17	ATV COBI FTC TDF
583-024	M	33.5	1021 (49%)	<20	5.7	5.6	EVG COBI FTC TAF

*This assay is performed with the Roche COBAS AmpliPrep/COBAS TaqMan HIV Test. [†]From the date of diagnosis [‡]Complete virological and immunological intestinal analyses were not performed.

(*2*, *34*). Although CD4$^+$ T cell depletion was less marked in the lymphoid aggregates, HIV-1 RNA (as measured by in situ hybridization) was mainly detected in the lymphoid aggregates (*2*, *34*). These data suggested to us that the intestinal lamina propria and lymphoid aggregates have distinct immunological and virological readouts during HIV-1 infection. Therefore, in addition to the LC, we decided to perform full colonoscopies to biopsy the TI enriched for lymphoid aggregates and comprehensively defined B and T cell subsets as detailed below.

We first defined a flow cytometric strategy to identify the known B cell subsets and plasma cells in intestinal mucosa and in circulation, identifying plasma cells as live CD45$^+$CD38^{hi}CD27$^+$ cells and nonplasma cell B cells as live CD45$^+$CD38$^-$CD19$^+$ cells. Among nonplasma cell B cells, naïve B cells were defined as CD45$^+$CD38$^-$CD19$^+$IgD$^+$IgM$^+$ cells, whereas switched memory (SM) B cells were defined as CD45$^+$CD38$^-$CD19$^+$IgD$^-$IgM$^-$ cells (fig. S2).

The TI contains more lymphoid aggregates and therefore more nonplasma cell B cells, whereas the LC harbors more lamina propria lymphocytes and therefore mostly differentiated plasma cells (*5*). In our patients, there was a clear dichotomy in the effects of anti-α4β7 therapy between the TI and LC, reflecting distinct cellular composition of these two intestinal sites. For example, we observed a marked decrease in nonplasma cell B cells (CD19$^+$CD38$^-$) in the TI of all five patients by flow cytometry. In contrast, in the LC that contains fewer nonplasma B cells, the decrease was less pronounced (Fig. 1, A and B). Among B cell subsets, both naïve and SM B cells were reduced in the TI after therapy. Again, in the LC with fewer total B cells, decrease in B cell subsets was less pronounced. (Fig. 1C). Among GI plasma cells, no decrease was noted in either the TI or LC (Fig. 1, A and B).

In circulation, although there was interindividual variability, we observed an early increase in all nonplasma cell B cells and in circulating plasmablasts (defined as Ki67$^+$CD38$^+$CD27$^+$IgD$^-$CD19$^{+/int}$ cells; fig. S2) at week 2 after VDZ initiation. No statistically significant changes were observed over the course of 30 weeks of VDZ treatment (*P* = 0.43; Fig. 1D).

Next, we compared B cell composition between a cohort of healthy volunteers, patients with HIV-1 alone (without IBD), and the VDZ-treated HIV-1$^+$ patients. Compared to healthy volunteers, a significant decrease was noted in total nonplasma cell B cells in the TI after VDZ treatment (*P* < 0.05; Fig. 1E). This was associated with a reduced frequency of naïve B cells, although changes in SM B cells and plasma cells in the TI were not significantly different between normal volunteers and VDZ-treated patients (*P* = 0.19 and *P* = 0.07, respectively). In contrast to the TI, we did not observe significant changes in total nonplasma cell B cells (*P* = 0.12), B cell subsets (naïve B cells, *P* = 0.15; SM B cells, *P* = 0.11), or plasma cells (*P* = 0.17) in the LC after VDZ treatment, when compared to healthy volunteers (Fig. 1E). All B cell subsets were comparable in the TI and LC between HIV-infected controls and HIV-infected IBD patients before VDZ (Fig. 1E). Finally, no significant changes in circulating B cell subsets were noted after VDZ treatment when compared to healthy volunteers or HIV controls (Fig. 1F). Overall, all five patients presented a major decrease in nonplasma cell B cells (including both naïve and memory subsets) in the TI with anti-α4β7 therapy.

Anti-α4β7 therapy results in attrition of lymphoid aggregates within the GI tract
Next, we quantified GI B cells by immunohistochemistry (IHC) to confirm and further define the anatomical compartments showing changes in B cells after VDZ. Because CD19 also identifies a subset of plasma cells, we used CD20 staining to quantify nonplasma cell B cells per unit area in lymphoid aggregates and lamina propria in the TI and LC. Lymphoid aggregates were noted after treatment in four of five subjects in the TI and two of five subjects in LC. In the TI, there was a pronounced CD20$^+$ B cell reduction in TI-associated lymphoid aggregates after VDZ in all four of five subjects, where lymphoid aggregates were detectable before treatment. In the LC, marked reduction in lymphoid aggregate–associated B cells was noted in one subject, whereas in the other, the reduction was more modest (Fig. 2B). VDZ treatment induced a reduction in lamina propria B cells in the TI and had a variable effect on lamina propria B cells in the LC (Fig. 2, A and B, and fig. S3).

Having observed a significant decrease in nonplasma cell B cells in the TI, we hypothesized that anti-α4β7 therapy has a pronounced effect on lymphoid aggregates. To define lymphoid aggregates within tissue, we used IHC and quantified the surface area covered by lymphoid aggregates in each of the tissue sections before and after VDZ (pathologists were blinded to the identity of the samples). In every subject, we observed a decrease in the percentage of total tissue surface covered by lymphoid aggregates after VDZ in the TI (from 24.1 ± 19.3% on average to 4.1 ± 2.9%; Fig. 2, C and D). Again, more variability was observed in the LC (from 3.8 ± 3.6% on average to 3.9 ± 4.5%), likely because lymphoid aggregates are less pronounced in the LC compared to the TI (*5*). To validate the IHC data, we performed immunofluorescence microscopy to examine B and T cell populations in the lymphoid aggregates versus the lamina propria. Consistent with the other findings, in this study, we found a significant decrease in number and size of lymphoid aggregates after VDZ (*P* < 0.001; Fig. 2, E and F).

To better understand the attrition of lymphoid aggregates, we examined for cellular proliferation using Ki67. As described previously, Ki67$^+$ cells were predominantly found in the lymphoid aggregates (*35*). We did not observe a significant decrease in Ki67$^+$ cells after VDZ (TI, *P* = 0.64; LC, *P* = 0.65), suggesting that lack of cell proliferation was likely not responsible for the attrition of lymphoid aggregates (fig. S4).

Next, we asked whether cellular apoptosis was responsible for the attrition of lymphoid aggregates by examining for apoptotic bodies by histology. As a result of negative selection of low-affinity and autoreactive B cells, apoptotic cells are present physiologically within the germinal centers of lymphoid aggregates (*36*). Accordingly, we found apoptotic cells within the lymphoid aggregates before VDZ, as shown in fig. S5. We did not observe an increase in apoptotic cells after VDZ (fig. S5).

Overall, we found profound and consistent changes of the lymphoid aggregates of the TI after VDZ therapy. They were substantially decreased in number and size, and they contained fewer CD20$^+$ B cells.

Anti-α4β7 therapy results in a decrease in naïve CD4$^+$ T cells in the TI
SIV macaque studies have demonstrated that anti-α4β7 therapy in combination with early cART enables better reconstitution of CD4$^+$ T cells in the colonic mucosa compared to cART alone (*27*). We therefore investigated the impact of VDZ on T cell subsets, including CD4$^+$ and CD8$^+$ T cells in the GI tract and in circulation. In the TI, there was a trend toward an increased frequency of total CD3$^+$ T cells after VDZ treatment, whereas CD3$^+$ T cell changes in the LC after VDZ were variable (Fig. 3A). Among T cell subsets, there was no significant change in the CD4/CD8 ratio in the TI (*P* = 0.24) or the LC (*P* = 0.19) in each of the patients after VDZ (Fig. 3B). When compared to healthy
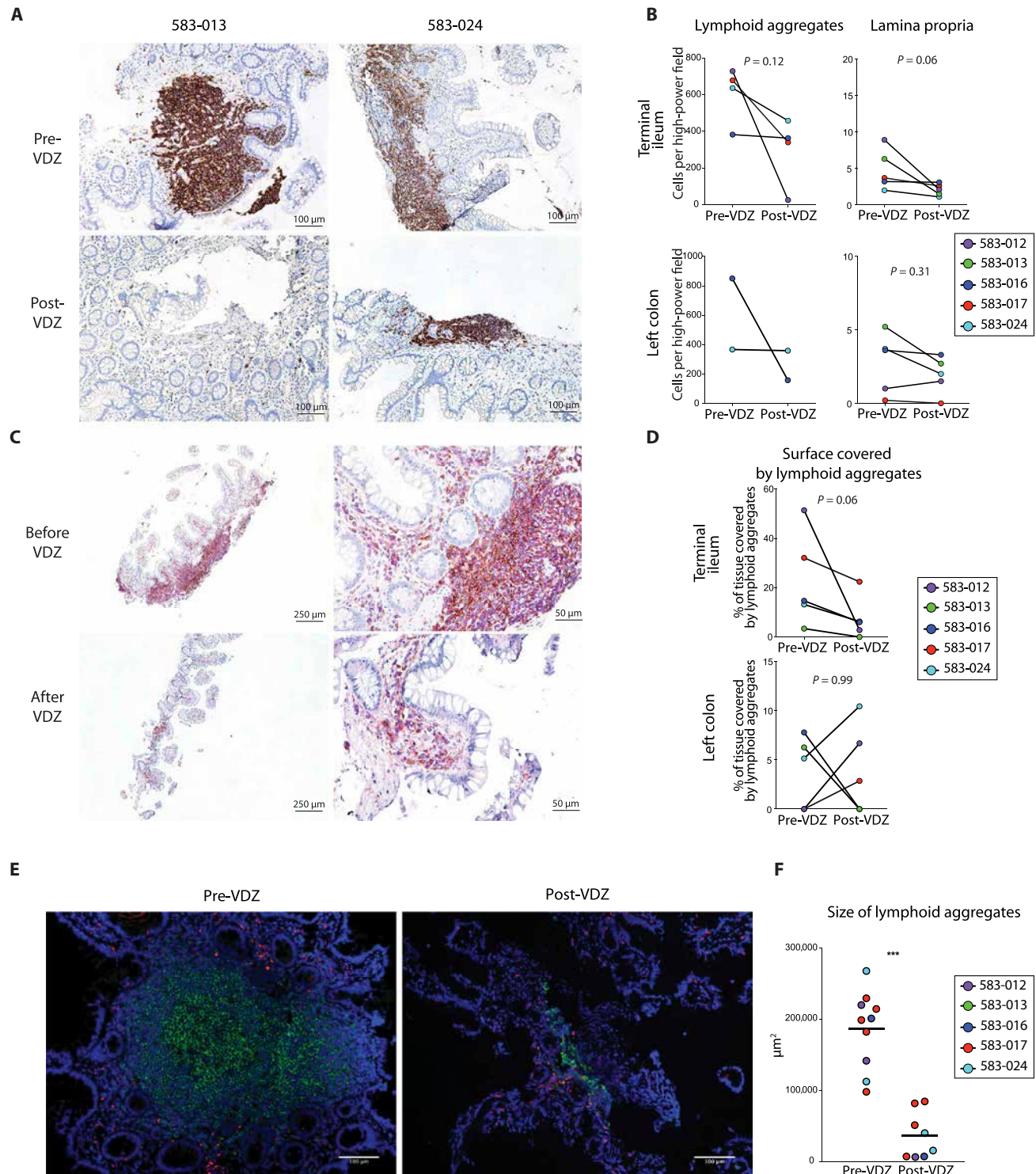
Fig. 1. Anti-α4β7 therapy decreases the frequency of B cell subsets in the TI. (**A** to **C**) Frequency of B cells and plasma cells in the GI tract before and after VDZ therapy. (A) Representative flow cytometry plots showing the expression of CD19 and CD38 among live, CD45^{+} cells derived from the TI (top panels) and LC (bottom panels) of subject 583-017, before VDZ and at week 30 after VDZ. (B) Plots comparing the change in frequency of nonplasma cell (CD19^{+}CD38^{−}) B cells and plasma cells (CD45^{+}CD38^{++}CD27^{+}) in the TI (top) and LC (bottom) between before and after VDZ treatment. (C) Plots demonstrating changes in the frequency of naïve (CD45^{+}CD19^{+}CD10^{−}CD38^{−}IgM^{+}IgD^{+}) and SM B cells (CD45^{+}CD19^{+}CD10^{−}CD38^{−}IgM^{−}IgD^{−}) in TI (top) and LC (bottom). (**D**) Change in the frequency of nonplasma cell B cells, B cell subsets, and plasma cells in the blood after VDZ therapy. In (A) to (D), each of the patients is represented with a unique color code. (**E**) Group comparisons in the frequency of B cell subsets and plasma cells within the TI and the LC. (**F**) Group comparisons in the frequency of B cell subsets and plasma cells in the peripheral blood. In (E) and (F), healthy volunteers (*n* = 11) are shown in red, HIV controls (*n* = 10) in blue, HIV-IBD subjects (*n* = 5) before VDZ in green, and HIV-IBD subjects after VDZ in gray. Two-tailed *t* test was performed to compare the different groups, and two-tailed paired *t* test was used to compare pre- and post-VDZ time points in the HIV-IBD patients. Statistical values are as indicated. *P < 0.05. NS, not significant.

Fig. 2. Anti-α4β7 therapy results in a significant attenuation of lymphoid aggregates, most pronounced in the TI. (**A**) Representative ×10 magnification images of TI-derived biopsies immunostained for CD20 expression (brown) in two subjects (583-013 and 583-024) before (top panels) and after (bottom panels) VDZ. (**B**) Quantitative analyses of CD20^{+} B cells in the TI (top) and LC (bottom). Cell frequency was determined separately in lymphoid aggregates (left) and in lamina propria (right). (**C**) Representative images from subject 583-017 showing dual immunohistochemical staining with CD19 (pink) and CD4 (brown) before (top) and after (bottom) VDZ. Original magnification, ×4 (left panel) and ×20 (right panel). (**D**) Percentage of tissue covered by lymphoid aggregates in the TI (top) and LC (bottom) in each of the subjects. (**E**) Representative immunofluorescence image showing the expression of CD3 (red), CD20 (green), and 4′,6-diamidino-2-phenylindole (blue) from the TI of subject 583-024, before (left panel) and after VDZ (right panel). Original magnification, ×10. (**F**) Cumulative data showing size of lymphoid aggregates between before and after VDZ treatment. In (B), (D), and (F), each of the patients is represented with a unique color code. Statistical values are as indicated. Wilcoxon matched-pairs signed-rank test and two-tailed *t* test (F) were used for statistical comparisons. Statistical values are as indicated. ***$P < 0.0005$.
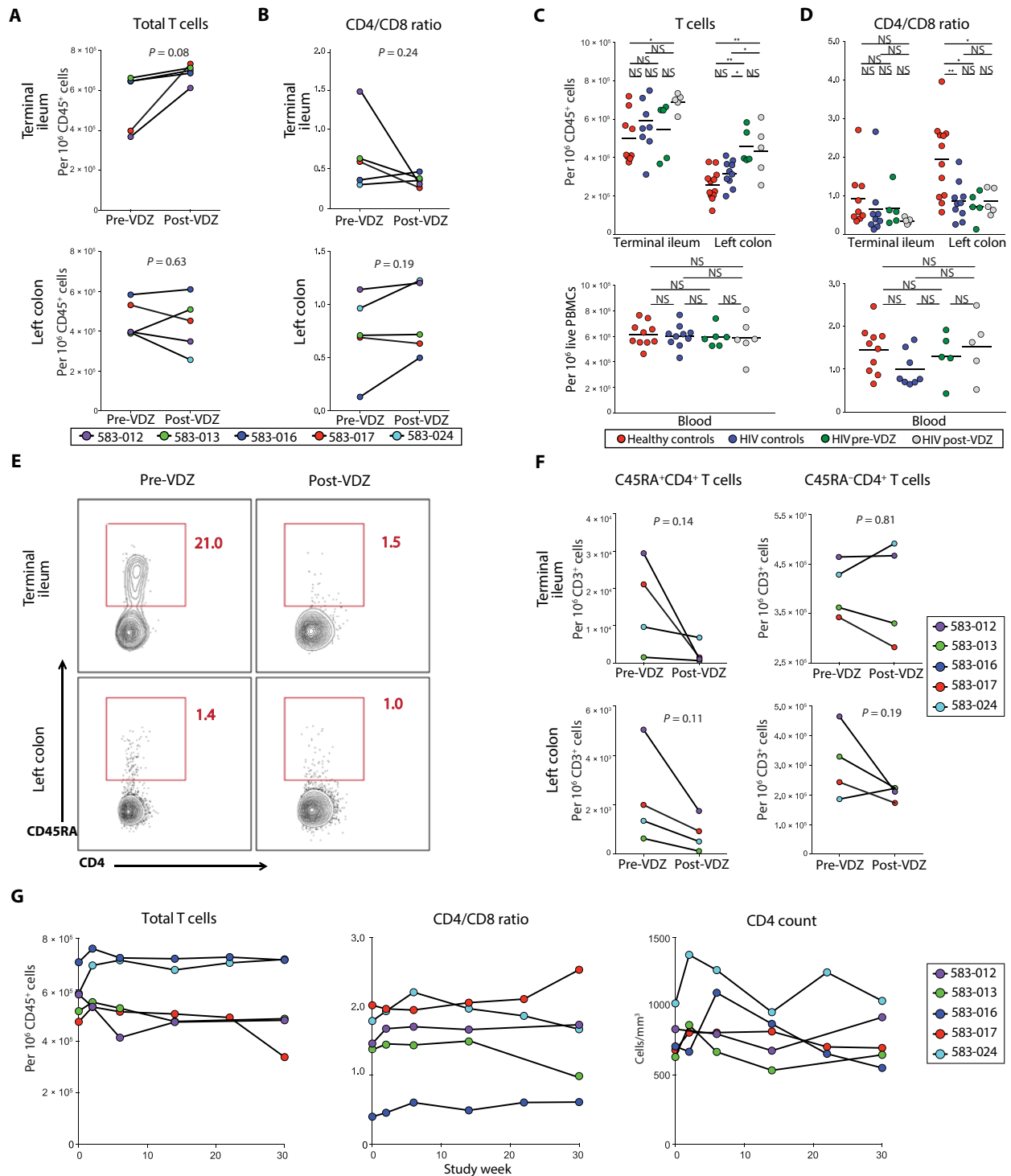
Fig. 3. Anti-α4β7 therapy results in a decrease in naïve CD4+ T cells in the TI. (**A** and **B**) Frequency of T cells in the GI tract before and after VDZ therapy. (A) Frequency of total CD3+ T cells and (B) CD4/CD8 T cell ratio in the TI (top panels) and LC (bottom panels). Each of the patients is represented with a unique color code, and statistical values are indicated. (**C** and **D**) Group comparisons between the frequency of T cells (C) and CD4/CD8 ratio (D) in the GI tract (top panels) and peripheral blood (bottom panels). Healthy volunteers (*n* = 12) are shown in red, HIV alone controls (*n* = 10) in blue, HIV-IBD subjects before VDZ (*n* = 5) in green, and HIV-IBD subjects after VDZ (*n* = 5) in gray. (**E** and **F**) Frequency of naïve and memory CD4+ T cells in the GI tract before and after VDZ. (E) Representative flow cytometry plots showing the expression of CD45RA on CD45+CD3+CD4+ T cells derived from the TI (top panels) and LC (bottom panels) of subject 583-024 before VDZ and at week 26 after VDZ. (F) Cumulative data showing changes in CD45RA+ (left) and CD45RA−CD4+ T cell subsets (right) within the TI (top panels) and LC (bottom panels). Notably, CD45RA+ staining on CD4+ T cells was available for four of five patients. (**G**) Cumulative data showing changes in the frequency of circulating total CD3+ T cells, CD4/CD8 ratio, and total CD4+ T cells during VDZ therapy for each patient. In (F) and (G), each of the patients is represented with a unique color code, and statistical values are indicated. *P < 0.05, **P < 0.005. Two-tailed *t* test was performed to compare the different groups, and two-tailed paired *t* test was used to compare pre- and post-VDZ time points in the HIV-IBD patients.

volunteers, there was a significant increase in CD3^{+} T cells in the TI ($P < 0.05$) and the LC ($P < 0.01$) after VDZ (Fig. 3C, top panel). In contrast to total T cells, there was no significant change in the CD4/CD8 ratios in the TI after VDZ when compared to healthy volunteers ($P = 0.06$). HIV-1–infected subjects had significantly reduced CD4/CD8 ratio in the LC when compared to healthy volunteers ($P < 0.01$), consistent with the published literature (37). However, CD4/CD8 ratio in the LC did not change significantly after VDZ treatment ($P = 0.19$; Fig. 3D, top panel). In the LC, the HIV-IBD patients (before and after VDZ) had higher frequencies of CD3^{+} T cells (Fig. 3C). Although LC biopsies were obtained from histologically uninflamed areas (fig. S1), we cannot exclude IBD as a cause of increased frequencies of CD3^{+} T cells in the LC. Finally, among circulating T cells, there were no significant differences in the total T cells or CD4/CD8 ratios between healthy volunteers, HIV controls, or the study subjects before or after VDZ treatment (Fig. 3, C and D, bottom panels).

Within T cells, there was no significant change in the total numbers of CD4^{+} T cells as quantified by IHC (TI lamina propria, $P = 0.46$; LC lamina propria, $P = 0.17$; fig. S6). Among CD4^{+} T cell subsets, there were no significant changes in the memory CD4^{+} T cells (CD3^{+}CD4^{+}CD45RA^{−}) after VDZ in the TI or LC ($P = 0.81$ and $P = 0.19$, respectively; Fig. 3, E and F). In contrast to memory CD4^{+} T cells, we noticed a decrease in naïve CD4^{+} T cells (CD3^{+}CD4^{+}CD45RA^{+}) in the TI and LC after VDZ, although the changes were not statistically significant (TI, $P = 0.14$; LC, $P = 0.11$; Fig. 3, E and F). As shown in fig. S7, naïve T cells express α4β7 at an intermediate level which potentially enables naïve T cell entry into the GI tract as has been documented in seminal studies by Butcher *et al.* (6, 8, 38). Thus, an intermediate level of expression of α4β7 may underlie the impact of VDZ on this population. Naïve T cells reside within the lymphoid aggregates, whereas memory T cells are largely distributed in the intestinal lamina propria (5). These data again demonstrate a previously unappreciated effect of anti-α4β7 therapy on lymphoid aggregates in the GI tract. In contrast, in circulation, although there was a short-term rise in total CD3^{+} T cells, CD4/CD8 ratios, and absolute CD4^{+} T cell counts at week 2 after treatment, over the course of 30 weeks, these counts tended to return to baseline (Fig. 3G).

In circulation, because α4β7 was almost completely saturated by VDZ, β7 integrin was used as a surrogate marker of α4β7 (fig. S8). There was a significant rise in β7^{hi}CD45RA^{−}CD4^{+} T cells, shown to be extremely susceptible to HIV-1 infection (23) at week 2, sustained over the duration of therapy (Fig. 4, A and B).

To further define the impact of VDZ on T cell subsets, we performed mass cytometry (CyTOF), allowing resolution of dozens of markers on a single cell (39, 40). Cryopreserved peripheral blood mononuclear cell (PBMC) samples from each of the patients were studied at baseline (week 0), week 2, and week 30. The data generated were analyzed using a combination of manual gating based on the expression of canonical markers and dimensionality reducing data visualization using visualization of *t*-distributed stochastic neighbor embedding (41) based on all phenotypic markers (Fig. 4C). To define major CD4^{+} T cell subsets including naïve, central memory (CM), effector memory (EM), terminally differentiated effector memory (EMRA) cells, regulatory T (T$_{reg}$) cells, and αE[+] (CD103) populations, we manually gated cells based on the expression of canonical markers as shown in the heat map in Fig. 4C. We then used viSNE analyses to examine the expression of β7 integrin on each of the major CD4^{+} T cell subsets and further defined the expression of multiple phenotypic markers including CD29 (β1 integrin), CD38

(activation), and CD161 (T helper 17 cells; Fig. 4D). Although we did not observe population-level differences among naïve, EMRA, and T$_{reg}$ cells, there was a significant increase in the frequency of β7^{+}CM CD4^{+} T cells ($P < 0.05$ at week 2) and β7^{+}EM CD4^{+} T cells ($P = 0.01$ at week 30) in circulation after VDZ (Fig. 4E). Lack of population-level changes in T cell subsets was also observed using flow cytometry (fig. S9). Because of limited sample availability, CyTOF analyses could not be performed on GI-resident T cells in the present study.

Because the β7 integrin can dimerize with either α4 or αE (fig. S10), we examined the contribution of αEβ7^{+} cells in the expansion of peripheral β7^{+} cells. αEβ7^{+} cells had high expression of β7 integrin (Fig. 4D). In every patient, and most notably in 583-012 and 583-017, there was an increase in αEβ7^{+} cells in circulation after VDZ (Fig. 4E). In confirmation of the CyTOF data, conventional flow cytometry also revealed an expansion of CD45RA^{−}αEβ7^{+} cells in circulation (Fig. 4, F and G). That said, because αEβ7^{+} cells account for a minority (~3%) of the β7^{+} cells (fig. S10), we posit that the overall expansion of β7^{+} cells in circulation was due to α4β7.

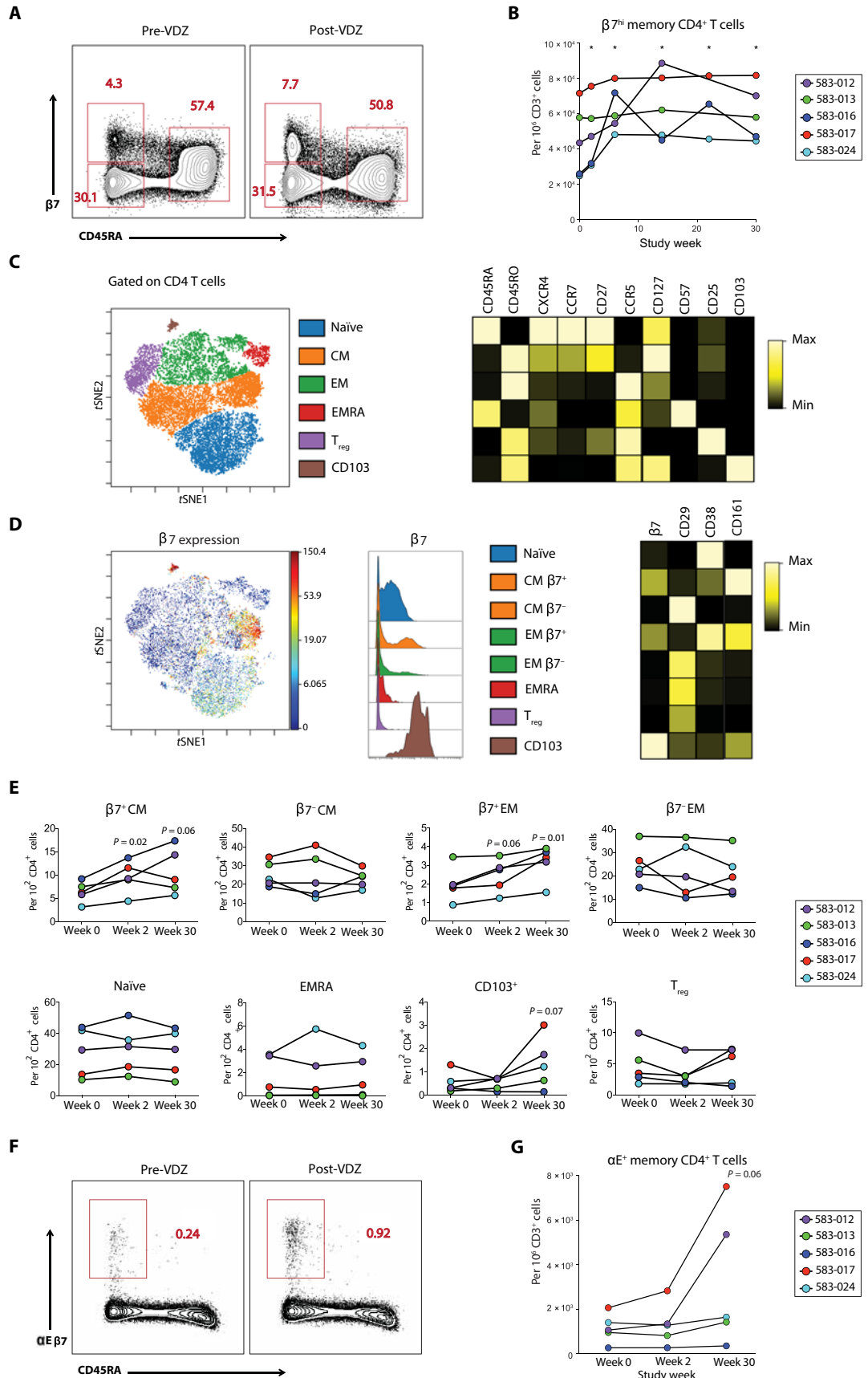### Anti-α4β7 therapy is associated with a decrease in activated CD4^{+} T cells in the TI

Cellular activation, causally related to susceptibility to HIV-1 infection and HIV-1 latency (42) and an independent marker of disease progression (43, 44), is significantly greater in the GI tract than that in the peripheral blood of patients with HIV-1 infection (34). To determine the impact of anti-α4β7 therapy on immunological activation in the GI tissue and peripheral blood, we assessed for the expression of CD38 on CD4^{+} and CD8^{+} T cells (defined in fig. S11). A significant reduction in the frequency of CD4^{+}CD38^{+} T cells was seen in the TI in all five subjects after VDZ treatment ($P = 0.01$; Fig. 5, A and B). In the LC, CD4^{+}CD38^{+} cells decreased in four of five subjects. Among CD8^{+} T cells, changes in CD8^{+}CD38^{+} cells were not significant in the TI ($P = 0.17$) or the LC ($P = 0.65$; Fig. 5, A and B). In the peripheral blood, although individual subjects showed a reduction in CD4^{+}CD38^{+} cells and CD8^{+}CD38^{+} cells, there was variability as a group, and the results did not reach significance ($P = 0.88$ CD4^{+}CD38^{+} cells and 0.68 for CD8^{+}CD38^{+} cells at week 30; Fig. 5C). The change of the frequency of circulating CD38^{+}HLA-DR^{+} double-positive CD4^{+} and CD8^{+} T cells was also variable between individuals, and no significant differences were noted after 30 weeks of treatment ($P = 0.25$ for CD4^{+} T cells and 0.68 for CD8^{+} T cells at week 30; fig. S12). To obtain a better resolution on the major CD4^{+} T cell subsets, we defined the expression of CD38 on memory and naïve cell subsets using CyTOF as detailed in Fig. 4 and segregated cells by β7 expression. As shown in Fig. 5D, β7^{+}CM CD4^{+} T cells and naïve CD4^{+} T cells had a significant reduction in CD38 expression after VDZ, seen at week 2 (β7^{+}CM CD4^{+} T cells, $P = 0.02$; naïve CD4^{+} T cells, $P = 0.04$) and week 30 (β7^{+}CM CD4^{+} T cells, $P = 0.02$; naïve CD4^{+} T cells, $P = 0.02$). When compared with healthy volunteers and HIV controls, there was a nonstatistically significant reduction in CD4^{+}CD38^{+} cells in the TI after VDZ treatment. In contrast, among circulating T cells, the frequency of bulk CD4^{+}CD38^{+} and CD8^{+}CD38^{+} cells was remarkably similar between healthy volunteers, HIV controls, and VDZ-treated subjects (Fig. 5D).

Anti-α4β7 therapy results in early changes in natural killer cell composition and activation that equilibrates over time

Natural killer (NK) cells play a critical role in viral immunity including HIV with multiple lines of evidence supporting a role for both

Fig. 4. Anti-α4β7 therapy is associated with alterations in the number and phenotype of β7⁺ cells in circulation. (**A** and **B**) Frequency of β7^{hi} memory T cell subsets in the peripheral blood before and after VDZ as measured by flow cytometry. (A) Representative flow cytometry plots from subject 583-017 comparing the expression of β7 integrin and CD45RA on circulating CD4⁺ T cells before VDZ and at week 30 after VDZ. Three distinct populations are defined: β7^{hi}CD45RA⁻, β7⁻CD45RA⁻, and β7^{int}CD45RA⁺. (B) Cumulative data showing changes in circulating β7^{hi}CD45RA⁻CD4⁺ T cells during VDZ therapy for each patient. (**C** to **E**) CyTOF analyses to define alterations in the frequency of immune cell subsets after VDZ. (C) *t*-distributed stochastic neighbor embedding (*t*SNE) analyses showing the major T cell subsets including naïve, CM, EM, EMRA, T$_{reg}$ cells, and αE⁺ (CD103) cells. These populations were manually gated on the basis of the expression of canonical markers as shown in the heat map on the right. (D) β7 integrin expression on each of the immune populations defined in (C). The expression of CD29, CD38, and CD161 on each of the cellular subsets is shown by a heat map. (E) Frequency of the indicated cell populations by CyTOF for each of the patients at baseline, week 2, and week 30. (**F** and **G**) Flow cytometric evaluation of αE⁺ (CD103) cells after VDZ. (F) Representative flow cytometry plots from subject 583-017 comparing the expression of αE (CD103) and CD45RA on circulating CD4⁺ T cells before VDZ and at week 30 after VDZ. (G) Cumulative data showing changes in circulating αEβ7⁺CD45RA⁻CD4⁺ T cells during VDZ therapy for each patient. In (E) and (G), each of the patients is represented with a unique color code. Significance values are as indicated in the figure. Two-tailed *t* test was performed to compare the different groups, and two-tailed paired *t* test was used to compare pre- and post-VDZ time points in the HIV-IBD patients.
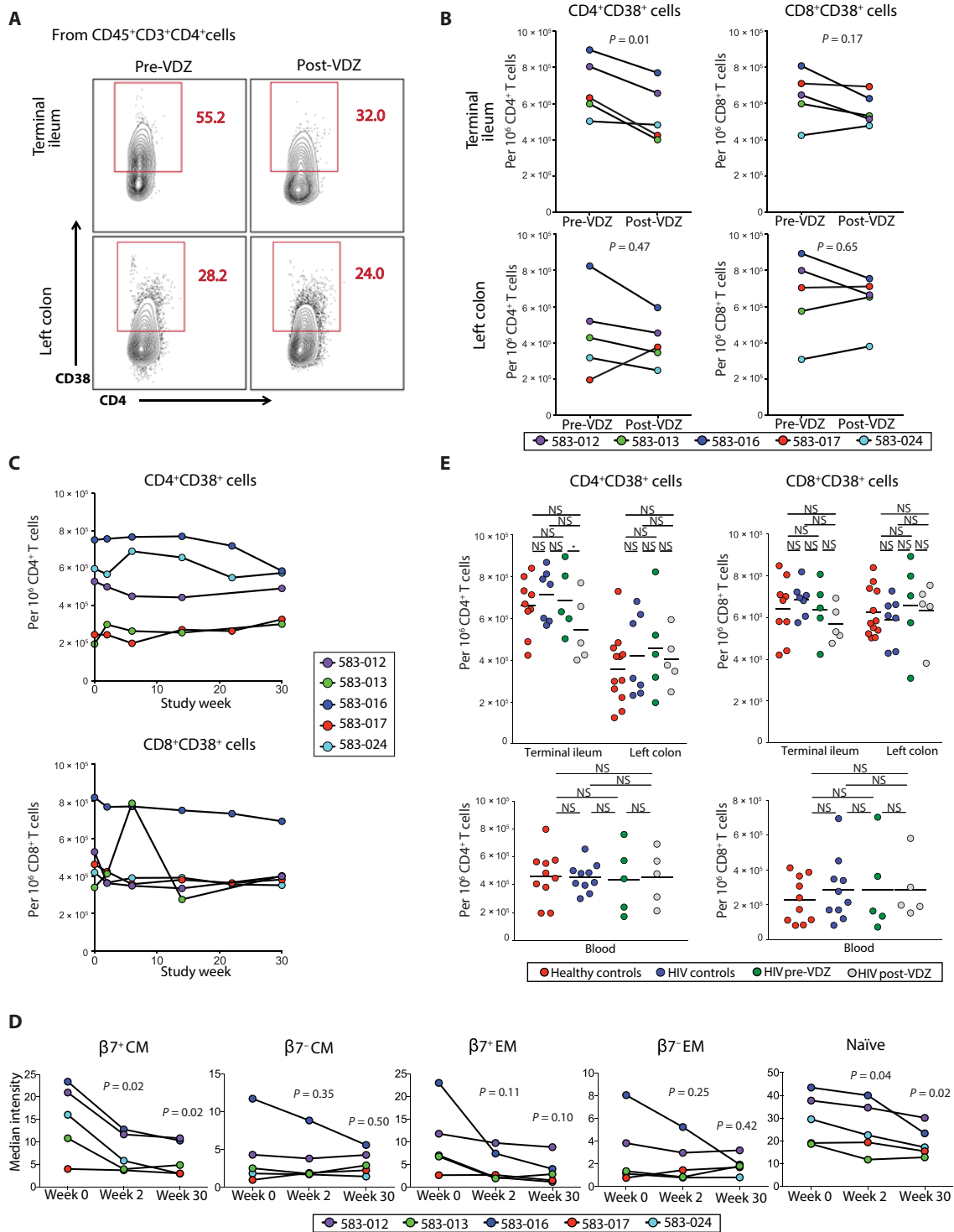
Fig. 5. Anti-α4β7 therapy is associated with a decrease in activated CD4⁺ T cells in the TI. (**A** and **B**) Frequency of activated T cells in the GI tract before and after VDZ. (A) Representative flow cytometry plots showing the expression of CD38 on live CD45⁺CD3⁺CD4⁺ T cells derived from TI (top) and LC (bottom) in subject 583-013 before VDZ and at week 26 after VDZ. (B) Cumulative data showing changes in the number of CD4⁺CD38⁺ T cells (left) and CD8⁺CD38⁺ T cells (right) in the TI (top panels) and LC (bottom panels) in each of the study subject after VDZ. (**C**) Frequency of CD4⁺CD38⁺ T cells (top) and of CD8⁺CD38⁺ T cells (bottom) in the peripheral blood throughout the study. (**D**) CyTOF analyses showing the median intensity of expression of CD38, compared for the indicated cell population on each of the patients at baseline, week 2, and week 30. In (B) to (D), each of the patients is represented with a unique color code. Significance values are as indicated in the figure. (**E**) Group comparisons between the frequency of CD4⁺CD38⁺ T cells (top left) and CD8⁺CD38⁺ cells (top right) in the GI tract and in the peripheral blood (bottom panels). Healthy volunteers (*n* = 12) are shown in red, HIV controls (*n* = 10) in blue, HIV-IBD subjects before VDZ (*n* = 5) in green, and HIV-IBD subjects after VDZ (*n* = 5) in gray. Two-tailed *t* test was performed to compare the different groups, and two-tailed paired *t* test was used to compare pre- and post-VDZ time points in the HIV-IBD patients.

cytotoxic and regulatory functions in HIV-1 infection (*45*). Therefore, we analyzed the composition and the activation of NK cells at baseline, week 2, and week 30 after VDZ. We defined NK cells in three distinct subsets as follows: Cytolytic NK cells were defined as $CD56^{dim}CD16^{high}$ NK cells, cytokine-secreting NK cells as $CD56^{bright}CD16^{low}$ NK cells, and $CD56^{null}$ cells as $CD56^{low}CD16^{high}$ NK cells (Fig. 6A and fig. S13). We found that, in all patients, the frequency of circulating $CD56^{bright}CD16^{low}$ cytokine-secreting NK cells decreased at week 2 and increased back to a level similar to baseline at week 30 (Fig. 6B). No clear differences were seen in the two other subsets (Fig. 6, C and D) or in the subset of $CD56^+$ NK cells coexpressing CD8 (Fig. 6E)

We further looked at the expression of human leukocyte antigen–DR isotype (HLA-DR) and programmed cell death-1 (PD-1) on $CD56^{dim}$ cytolytic NK cells. An increase in the expression of HLA-DR was noted in four of five subjects at week 2, suggesting the activation of cytolytic NK cells after VDZ (Fig. 6F and fig. S14). Finally, the expression of PD-1 on $CD56^{dim}$ cytolytic NK cells also increased in four of five subjects at week 2 (Fig. 6G). Because of paucity of GI-derived cells, we were unable to assess for NK cell changes in the GI tract after VDZ. In summary, our data demonstrate changes in NK cell frequency and increased NK cell activation in circulation, early after anti-α4β7 therapy.

Anti-α4β7 therapy results in a variable effect on stimulated and unstimulated multiply spliced HIV-1 transcripts in blood-derived CD4$^+$ T cells

To study the impact of VDZ on the HIV reservoir, we used a combination of approaches assessing HIV-related measurement. All the patients continued on fully suppressive antiretroviral therapy for the course of this study. We observed a decrease in total HIV-1 DNA levels in sorted CD4$^+$ T cells derived from PBMCs in two of five patients. In addition, changes in proviral DNA were minimal in two of five patients and increased in one of five patients (total DNA, $P = 0.63$; integrated DNA, $P = 0.13$; Fig. 7A). In the TI, although there was a decrease in total and integrated HIV-1 DNA in three of five subjects, there was an increase in total and integrated HIV-1 DNA in two of five subjects and the changes were not statistically significant (total DNA, $P=0.31$; integrated DNA, $P = 0.44$; Fig. 7B, top panels). Similarly, the effect of VDZ treatment on HIV-1 DNA levels in the LC was variable and not significant (total DNA, $P = 0.52$; integrated DNA, $P = 0.60$; Fig. 7B, bottom panels). We did not detect HIV-1 RNA levels in unstimulated GI-derived CD4$^+$ T cells, and paucity of cell numbers made performance of quantitative viral outgrowth assays not feasible in this initial study.
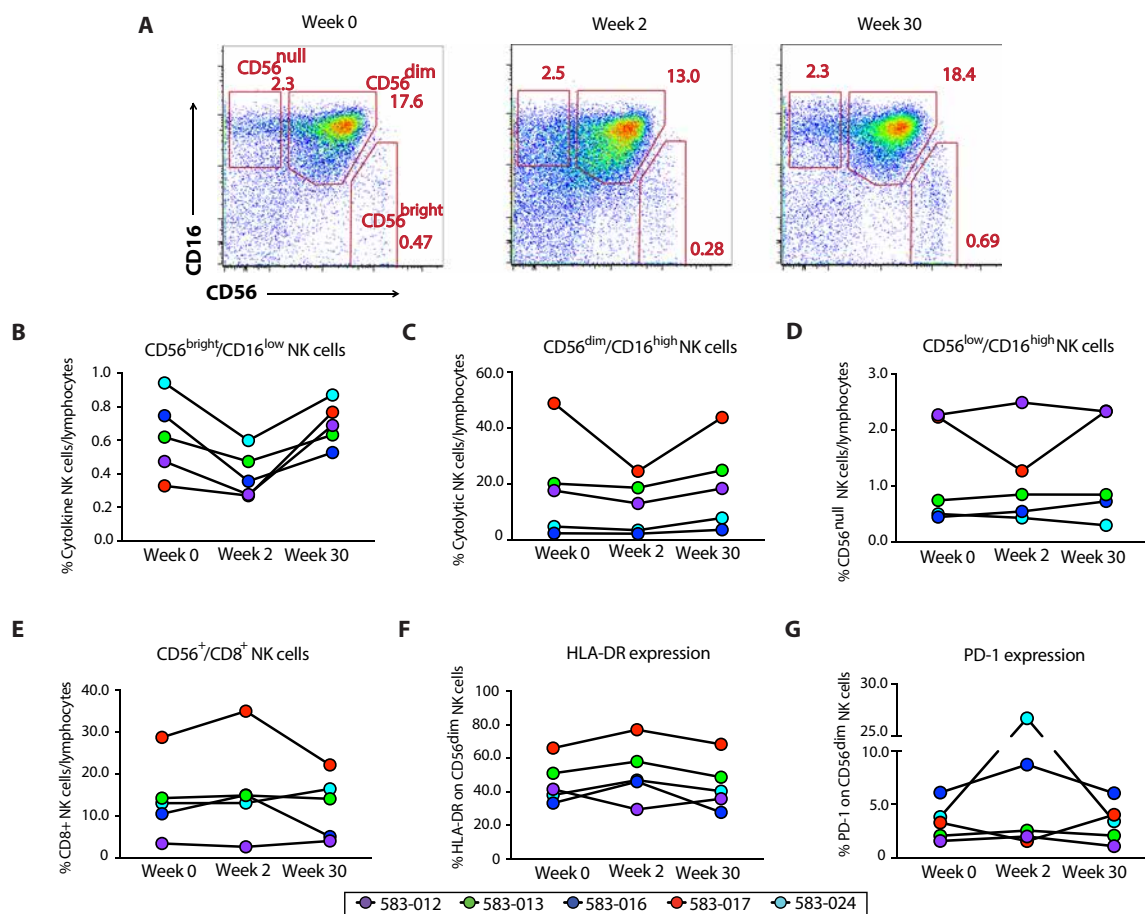

Fig. 6. Anti-α4β7 therapy results in the activation of circulating NK cell subsets. (**A**) NK cell phenotype at weeks 0, 2, and 30 of therapy with VDZ. After exclusion of dead cells, monocytes, B cells, and T cells, cytolytic NK cells were gated as $CD56^{dim}CD16^{high}$ NK cells, cytokine-secreting NK cells were gated as $CD56^{bright}CD16^{low}$ NK cells, and $CD56^{null}$ cells were gated as $CD56^{low}CD16^{high}$ NK cells. (**B** to **E**) Composite graphs representing frequency of cytokine-producing (B), cytolytic (C), and $CD56^{null}$ NK cells (D), as well as $CD56^+CD8^+$ NK cells (E) from each of the five subjects (color-coded) at weeks 0, 2, and 30 of therapy with VDZ. (**F** and **G**) Change in the expression of HLA-DR (F) and PD-1 (G) on cytolytic $CD56^{dim}CD16^{high}$ NK cells from five subjects (color-coded) at weeks 0, 2, and 30 of therapy with VDZ.
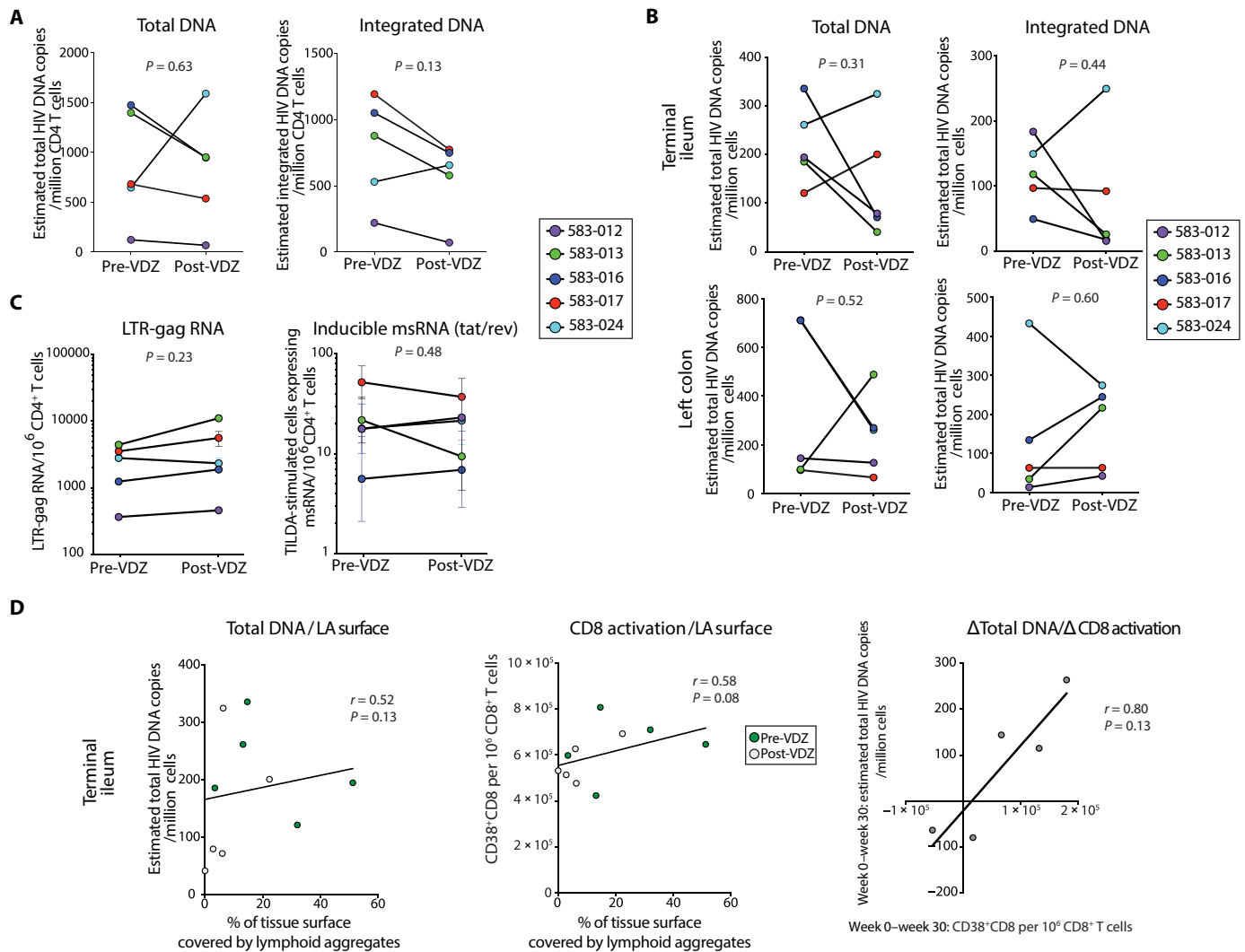
Fig. 7. Impact of anti-α4β7 therapy on HIV-1 levels in the peripheral blood and in the GI tract. (**A**) Estimated copies per million cells of total and integrated HIV DNA in sorted CD4^{+} T cells derived from PBMCs before and after VDZ. (**B**) Total and integrated HIV DNA in whole biopsies derived from the TI (top panels) and LC (bottom panels) before and after VDZ. DNA copy number was normalized per housekeeping gene (CD3) copy number. (**C**) HIV-1 long terminal repeat (LTR)–gag RNA in unstimulated bead-selected, circulating CD4 cells before VDZ and at week 30 after VDZ (left panel). In the right panel, frequency of cells with inducible multiply spliced RNA (msRNA; tat/rev), measured with the TILDA assay, is compared before and after VDZ. (**D**) Plots showing the linear regression line between various parameters in the TI mucosa. Left panel shows correlation between HIV total DNA within the TI and the percentage of tissue covered by lymphoid aggregates (LA). Middle panel shows the correlation between the frequency of CD8^{+}CD38^{+} activated cells and the surface covered by lymphoid aggregates in the TI. The right panel represents the correlation between the magnitude of week 0 to week 30 changes in total HIV-1 DNA levels and the frequency of CD8^{+}CD38^{+} cells. A positive number is representative of a decrease from week 0 to week 30. Correlation factors and *P* values were estimated with the Spearman correlation test. Two-tailed paired *t* test was used to compare before and after VDZ values. Statistical values are as indicated.

Tat/rev-induced limiting dilution assay (TILDA) was performed on peripheral blood-derived, bead-sorted CD4^{+} T cells before VDZ and at week 30 after treatment. In subjects 583-013 and 583-017, lower frequencies of cells with multiply spliced HIV RNA (tat/rev) were seen after treatment. In the absence of stimulation, LTR-gag transcripts were rare, and did not change significantly after VDZ (*P* = 0.23; Fig. 7C, left panel). Overall, in the face of ongoing cART, spliced and unspliced HIV-1 RNA in the blood showed variability and inconclusive overall effect of anti-α4β7 on markers of HIV-1 persistence (*P* = 0.48; Fig. 7C, right panel).

Further, we correlated the total DNA level in the TI with immunological parameters. We found a positive correlation (*r* = 0.52, *P* = 0.13) between the lymphoid aggregates and the DNA level, suggesting a po-

tential role of the TI lymphoid structures as viral reservoirs (Fig. 7D, left panel). In addition, the percentage of the GI surface covered by lymphoid aggregates in the TI correlated positively with CD8^{+} T cell activation (*r* = 0.58, *P* = 0.08; Fig. 7D, middle panel). Finally, we found a strong correlation (*r* = 0.8) between the magnitude of CD8^{+} T cell activation decrease and decrease in total DNA levels in the TI after VDZ (Fig. 7D, right panel).

DISCUSSION

A growing body of evidence has demonstrated that α4β7^{+}CD4^{+} T cells represent an early target for HIV-1 (*20*, *21*, *23*). Accordingly, NHP studies using an anti-α4β7 monoclonal antibody (mAb), that is a close

analog of VDZ, either before infection or in the context of SIV-infected animals receiving cART, have yielded promising and provocative results (*26*, *27*). This has prompted two ongoing phase 1 clinical trials of VDZ in HIV-infected subjects. However, the underlying mechanism(s) by which anti-α4β7 mAb therapy affected SIV pathogenesis remains unknown. Subjects coafflicted with HIV and IBD represent a unique opportunity to investigate the clinical utility of VDZ therapy in HIV disease. The goals of the present report were to determine the safety and tolerability of anti-α4β7 therapy in humans with HIV-1 infection. In addition, we performed detailed immunological analyses in the intestinal tissue and peripheral blood to provide insight into the mechanism(s) of action of this drug.

Data reported herein from six patients with chronic HIV-1 infection (five patients with detailed intestinal immunophenotyping) demonstrated that VDZ can be safely administered over extended periods of time. The only AEs recorded in our study were minor and self-limited, including episodes of upper respiratory infection as described previously (*28*).

To determine the immunological effects of VDZ on the GI tract, we examined both immune inductive sites (represented by lymphoid aggregates, concentrated in the TI) and effector sites (represented by lamina propria–associated lymphocytes). Notably, inductive sites such as the PPs harbor antigen-naïve T and B cells, whereas effector sites such as colonic lamina propria contain antigen-experienced memory T cells and plasma cells (*5*). Significantly reduced frequency of nonplasma cell B cell subsets (but not plasma cells) and naïve T cells (but not memory T cells) as assessed by flow cytometry after VDZ treatment drew our attention to the effect of anti-α4β7 therapy on lymphoid aggregates. In confirmation of our hypothesis that anti-α4β7 therapy targets lymphoid aggregates, we observed a marked attenuation of lymphoid aggregates in the course of treatment. These data, represent a previously unreported MOA of anti-α4β7 therapy and can be explained, in part, by the fact that lymphocyte homing to both inductive and effector sites, are α4β7-dependent (*6*, *38*). Although the existing literature has focused on drug therapeutic effects on memory cells homing to the effector compartment, we observed an even greater effect on the homing of naïve T and B cells to the inductive sites. Consistent with our observations, previous studies have reported variable effects of anti-α4β7 treatment on lamina propria lymphocytes (*10*). This may reflect redundant cellular homing pathways to the lamina propria and a more exclusive dependence on α4β7-MAdCAM interactions in homing to inductive sites (*6*, *8*, *38*). In support, we have observed a significant increase in β7^{hi} memory CD4^{+} T cells in circulation after VDZ therapy. Furthermore, NHP studies do not demonstrate hypocellularity in the lamina propria after VDZ treatment, which would be expected in the face of blocking cellular ingress (*46*). Finally, in one preclinical study where anti-α4β7 therapy was administered to cynomolgus monkeys and as many as 48 different sites were examined for drug effect, atrophy of PPs was observed after treatment, whereas no changes in the intestinal lamina propria were discernable (*47*). Viewed collectively, no significant change in CD4^{+} T cell frequencies in the lamina propria concurrent with an increase in β7^{hi} memory CD4^{+} T in circulation implies that CD4^{+} T cells are using redundant and perhaps α4β7-independent pathways of localizing to the GI lamina propria during VDZ therapy. Although α4β7 is best described as a "pan-GI" homing marker, it is likely that alternative and more specialized pathways exist. As an example, a G protein–coupled receptor, GPR-15, was recently described to mediate homing of regulatory T cells to the colon (*48*). A better understanding of α4β7-independent pathways of gut homing has important implications for IBD therapeutics and for HIV.

In addition to its effect on lymphoid aggregates, anti-α4β7 was associated with a decrease in the frequency of activated CD4^{+} T cell in the TI, which could be the consequence of either decreased activation or in reduced homing of activated cells. These data may also suggest an effect of immune stimulation by viral reservoirs in the TI. However, an obvious limitation here is the low number of patients—such observations would need to be validated in a larger data set. An additional point of interest and perhaps the subject of future investigation is the impact of therapy on the activation of CD56^{dim} cytolytic NK cells at week 2 after treatment. Unfortunately, we do not have tissue assessments of NK cell phenotype/function to better understand the impact of therapy on this important innate immune subset.

Virological effects of therapy, modest at best in the present study, were not unexpected in the face of ongoing, fully suppressive cART. In addition, in contrast to a SIV-macaque study (*9*), our data do not show clear differences between reduction of viral loads in the small and large intestines.

The patients described herein had concomitant IBD which could potentially confound the interpretation of our results. Given that anti-α4β7 therapy is not yet licensed for clinical use in HIV alone, this was a practical limitation for this study. That said, we believe that the impact of IBD on our analysis was minimal. The patients had very mild IBD. Furthermore, histological examination of tissues, arguably the gold standard for defining tissue inflammation, confirmed that the biopsied areas within the TI or the LC did not have mucosal inflammation.

Attenuation of lymphoid aggregates by anti-α4β7 therapy may have important implications for HIV-1 infection. It is well established that B cell follicles are a source of viral replication in the context of chronic infection (*49*). Notably, emerging data suggest that B cell follicles are a major source of replication-competent virus during cART (*50*) and may represent one barrier to viral eradication. Follicular DCs, physiological long-term stores of antigen for the development of high-affinity antibodies (*51*), accumulate a large reservoir of infectious extracellular HIV virions within the B cell follicles and serve as a major source of infectious virions in vivo (*52*–*54*). Virus can then be passed to follicular CD4^{+} T cells (including T follicular helper cells) that are highly susceptible to HIV-1 infection (*55*, *56*) through a variety of mechanisms including B cell lymphoma 6 (BCL-6)–mediated diminished expression of interferon-stimulated genes (*57*). Moreover, B cell follicles may be semi-immune privileged sites due to the inability of cytotoxic T cells lacking follicular homing molecule CXCR5 (*58*) to enter them (*59*). In accordance with this concept, it has been hypothesized that overcoming the immune privilege of lymphoid follicles may be the key to HIV cure efforts (*60*). Among the strategies being considered are the development of HIV-specific, CXCR5-expressing chimeric antigen receptor T cells (*61*), the use of bispecific antibodies (*62*), or treatment with latency reversal agents (LRAs) (*63*). Although significant attention has been paid to LRAs such as histone deacetylase inhibitors, protein kinase C agonists, and recombinant interleukin-15, to date, no LRA agent is known to specifically target the lymphoid aggregates. Here, unexpectedly, we have identified that a gut-specific immunotherapeutic agent can lead to the attrition of B cell follicles in the GI tract. This represents a potentially important tool in the HIV-1 cure effort. Given that the impact of anti-α4β7 therapy is primarily GI specific, it would possibly need to be combined with other agents to affect HIV-1 reservoirs in

both GI and non-GI sites. Another implication of the present report is the proposed duration of therapy. We contend that extended treatment with anti-α4β7 agents, either alone or in combination with other LRAs, will likely be required for a sustained impact on the lymphoid aggregates and should be considered in the design of future animal and human studies.

In summary, the present report provides evidence of safety and tolerability of anti-α4β7 therapy in HIV-infected subjects and provides insights into its effect on lymphoid aggregates. This activity may represent a new approach toward affecting persistent viral replication in gut tissues, which play a central role in HIV pathogenesis. In the ongoing efforts to develop an HIV cure, we believe that treatment with anti-α4β7 agents in combination with other LRAs may represent a new therapeutic approach.

MATERIALS AND METHODS
Study design
Patients were recruited from within a cohort of HIV-1–infected patients with concomitant IBD (64) being followed at the Icahn School of Medicine at Mount Sinai and its affiliated hospitals and clinics. Informed consent was obtained from all the participants. The study protocol was approved by the Mount Sinai institutional review board.

Six subjects with IBD and concomitant HIV-1 infection were prospectively enrolled into the study. Of these, ileocolonoscopy was performed before VDZ initiation in five subjects, and biopsies were obtained from the TI and LC. In one subject (583-004), colonoscopy could not be performed before treatment due to logistical reasons (the patient had already received the first dose of VDZ as the colonoscopy was being scheduled). Before VDZ, blood from this patient was stored, and she signed on to the study to be followed prospectively. Thus, although we have detailed safety data and immunological and virological data in circulation before and after VDZ on this patient, we have not included her in the analyses, lacking the pre-VDZ gut data. Full immunological and virological analyses are being reported on five subjects. VDZ infusions were administered following the U.S. Food and Drug Administration–approved protocol for IBD, including an induction phase with a 300 mg intravenous (iv) infusion at weeks 0, 2, and 6, subsequently followed by a maintenance phase with a 300 mg iv infusion every 8 weeks. Before each infusion, blood was collected for analysis. A repeat colonoscopy was performed on each of the five subjects between week 22 and week 30 after treatment. Although the patients continue to be on long-term follow-up and on VDZ therapy, for the present report, we are describing the effects of 30 weeks of VDZ therapy. All the patients continued stable and uninterrupted cART for the length of the study.

In addition, we recruited a cohort of healthy volunteers ($n = 12$) and a cohort of non-IBD patients identified during chronic HIV-1 infection who were all cART-treated and well controlled ($n = 10$; clinical details in tables S2 and S3). All healthy volunteers and chronic HIV-1 subjects underwent colonoscopy and phlebotomy for immunological analyses in the GI tract and peripheral blood, respectively. In addition to existing protocols in the lab, we studied the impact of collagenase digestion on the expression of CD4 receptor (fig. S15). Primary data are located in table S6.

Statistical analysis
Plots were drawn using GraphPad Prism software. Statistical significance of immunophenotyping and viral data was assessed using the two-sample paired Wilcoxon signed-rank test and two-tailed (paired) Student's *t* test when appropriate. Correlations were assessed using the Spearman test.

SUPPLEMENTARY MATERIALS
www.sciencetranslationalmedicine.org/cgi/content/full/10/461/eaau4711/DC1
Methodological details
Fig. S1. Histological examination of TI and LC before and after VDZ.
Fig. S2. B cell gating strategy.
Fig. S3. CD20 immunostaining of terminal ileal biopsies before and after VDZ.
Fig. S4. Change in the frequency of Ki67+ cells in GI tissue.
Fig. S5. Representative image of apoptotic bodies.
Fig. S6. CD4 quantification in biopsies of the TI and LC.
Fig. S7. Representative flow cytometry plots of showing the expression of α4β7 on naïve and memory CD4+ T cells in the peripheral blood of a healthy volunteer.
Fig. S8. Masking of α4β7 by VDZ and β7 as a surrogate marker of α4β7+ cells.
Fig. S9. Change in the frequency of CD4+ T cells subsets in circulation after VDZ.
Fig. S10. Expression of integrin α4 and αE on β7+ memory CD4+ T cells.
Fig. S11. Gating strategy to define the frequency of CD38+ "activated" CD4+ and CD8+ T cells in the GI tract.
Fig. S12. Change in the frequency of CD4+ and CD8+HLA-DR+CD38+ cells in circulation.
Fig. S13. Gating strategy for identifying NK cells.
Fig. S14. HLA-DR expression on cytolytic CD56dimCD16high NK cells.
Fig. S15. Impact of collagenase digestion on the frequency of intestinal CD4+ T cells.
Table S1. IBD-related clinical characteristics.
Table S2. Clinical characteristics of the healthy volunteers.
Table S3. HIV control cohort: Clinical characteristics.
Table S4. Flow cytometry antibodies.
Table S5. List of CyTOF reagents.
Table S6. Primary data.
References (65, 66)

REFERENCES AND NOTES
1. S. Mehandru, S. Dandekar, Role of the gastrointestinal tract in establishing infection in primates and humans. *Curr. Opin. HIV AIDS* **3**, 22–27 (2008).
2. S. Mehandru, M. A. Poles, K. Tenner-Racz, A. Horowitz, A. Hurley, C. Hogan, D. Boden, P. Racz, M. Markowitz, Primary HIV-1 infection is associated with preferential depletion of CD4+ T lymphocytes from effector sites in the gastrointestinal tract. *J. Exp. Med.* **200**, 761–770 (2004).
3. M. Guadalupe, E. Reay, S. Sankaran, T. Prindiville, J. Flamm, A. McNeil, S. Dandekar, Severe CD4+ T-cell depletion in gut lymphoid tissue during primary human immunodeficiency virus type 1 infection and substantial delay in restoration following highly active antiretroviral therapy. *J. Virol.* **77**, 11708–11717 (2003).
4. J. M. Brenchley, T. W. Schacker, L. E. Ruff, D. A. Price, J. H. Taylor, G. J. Beilman, P. L. Nguyen, A. Khoruts, M. Larson, A. T. Haase, D. C. Douek, CD4+ T cell depletion during all stages of HIV disease occurs predominantly in the gastrointestinal tract. *J. Exp. Med.* **200**, 749–759 (2004).
5. A. M. Mowat, J. L. Viney, The anatomical basis of intestinal immunity. *Immunol. Rev.* **156**, 145–166 (1997).
6. R. F. Bargatze, M. A. Jutila, E. C. Butcher, Distinct roles of L-selectin and integrins α4β7 and LFA-1 in lymphocyte homing to Peyer's patch-HEV in situ: The multistep model confirmed and refined. *Immunity* **3**, 99–108 (1995).
7. M. Iwata, A. Hirakiyama, Y. Eshima, H. Kagechika, C. Kato, S. Y. Song, Retinoic acid imprints gut-homing specificity on T cells. *Immunity* **21**, 527–538 (2004).
8. C. Berlin, E. L. Berg, M. J. Briskin, D. P. Andrew, P. J. Kilshaw, B. Holzmann, I. L. Weissman, A. Hamann, E. C. Butcher, α4β7 integrin mediates lymphocyte binding to the mucosal vascular addressin MAdCAM-1. *Cell* **74**, 185–195 (1993).
9. P. J. Santangelo, C. Cicala, S. N. Byrareddy, K. T. Ortiz, D. Little, K. E. Lindsay, S. Gumber, J. J. Hong, K. Jelicic, K. A. Rogers, C. Zurla, F. Villinger, A. A. Ansari, A. S. Fauci, J. Arthos, Early treatment of SIV+ macaques with an α4β7 mAb alters virus distribution and preserves CD4+ T cells in later stages of infection. *Mucosal Immunol.* **11**, 932–946 (2017).
10. S. Zeissig, E. Rosati, C. M. Dowds, K. Aden, J. Bethge, B. Schulte, W. H. Pan, N. Mishra, M. Zuhayra, M. Marx, M. Paulsen, A. Strigli, C. Conrad, D. Schuldt, A. Sinha, H. Ebsen, S. C. Kornell, S. Nikolaus, A. Arlt, D. Kabelitz, M. Ellrichmann, U. Lützen, P. C. Rosenstiel, A. Franke, S. Schreiber, Vedolizumab is associated with changes in innate rather than adaptive immunity in patients with inflammatory bowel disease. *Gut*, 10.1136/gutjnl-2018-316023 (2018).
11. R. S. Veazey, M. DeMaria, L. V. Chalifoux, D. E. Shvetz, D. R. Pauley, H. L. Knight, M. Rosenzweig, R. P. Johnson, R. C. Desrosiers, A. A. Lackner, Gastrointestinal tract as a

major site of CD4^{+} T cell depletion and viral replication in SIV infection. *Science* **280**, 427–431 (1998).

12. M. A. Poles, J. Elliott, P. Taing, P. A. Anton, I. S. Y. Chen, A preponderance of CCR5^{+} CXCR4^{+} mononuclear cells enhances gastrointestinal mucosal susceptibility to human immunodeficiency virus type 1 infection. *J. Virol.* **75**, 8390–8399 (2001).

13. H. L. Schieferdecker, R. Ullrich, H. Hirseland, M. Zeitz, T cell differentiation antigens on lymphocytes in the human intestinal lamina propria. *J. Immunol.* **149**, 2816–2822 (1992).

14. I. McGowan, J. Elliott, M. Fuerst, P. Taing, J. Boscardin, M. Poles, P. Anton, Increased HIV-1 mucosal replication is associated with generalized mucosal cytokine activation. *J. Acquir. Immune Defic. Syndr.* **37**, 1228–1236 (2004).

15. J. Arthos, C. Cicala, E. Martinelli, K. Macleod, D. Van Ryk, D. Wei, Z. Xiao, T. D. Veenstra, T. P. Conrad, R. A. Lempicki, S. McLaughlin, M. Pascuccio, R. Gopaul, J. McNally, C. C. Cruz, N. Censoplano, E. Chung, K. N. Reitano, S. Kottilil, D. J. Goode, A. S. Fauci, HIV-1 envelope protein binds to and signals through integrin α4β7, the gut mucosal homing receptor for peripheral T cells. *Nat. Immunol.* **9**, 301–309 (2008).

16. G. R. Nakamura, D. P. A. J. Fonseca, S. M. O'Rourke, A. L. Vollrath, P. W. Berman, Monoclonal antibodies to the V2 domain of MN-rgp120: Fine mapping of epitopes and inhibition of α4β7 binding. *PLOS ONE* **7**, e39045 (2012).

17. K. K. Peachman, N. Karasavvas, A.-L. Chenine, R. McLinden, S. Rerks-Ngarm, K. Jaranit, S. Nitayaphan, P. Pitisuttithum, S. Tovanabutra, S. Zolla-Pazner, N. L. Michael, J. H. Kim, C. R. Alving, M. Rao, Identification of new regions in HIV-1 gp120 variable 2 and 3 loops that bind to α4β7 integrin receptor. *PLOS ONE* **10**, e0143895 (2015).

18. C. Cicala, E. Martinelli, J. P. McNally, D. J. Goode, R. Gopaul, J. Hiatt, K. Jelicic, S. Kottilil, K. Macleod, A. O'Shea, N. Patel, D. Van Ryk, D. Wei, M. Pascuccio, L. Yi, L. McKinnon, P. Izulla, J. Kimani, R. Kaul, A. S. Fauci, J. Arthos, The integrin α4β7 forms a complex with cell-surface CD4 and defines a T-cell subset that is highly susceptible to infection by HIV-1. *Proc. Natl. Acad. Sci. U.S.A.* **106**, 20877–20882 (2009).

19. J. Ding, C. Tasker, P. Lespinasse, J. Dai, P. Fitzgerald-Bocarsly, W. Lu, D. Heller, T. L. Chang, Integrin α4β7 expression increases HIV susceptibility in activated cervical CD4+ T cells by an HIV attachment-independent mechanism. *J. Acquir. Immune Defic. Syndr.* **69**, 509–518 (2015).

20. V. R. Joag, L. R. McKinnon, J. Liu, S. T. Kidane, M. H. Yudin, B. Nyanga, S. Kimwaki, K. E. Besel, J. O. Obila, S. Huibner, J. O. Oyugi, J. Arthos, O. Anzala, J. Kimani, M. A. Ostrowski; Toronto HIV Research Group, R. Kaul, Identification of preferential CD4^{+} T-cell targets for HIV infection in the cervix. *Mucosal Immunol.* **9**, 1–12 (2016).

21. M. Kader, X. Wang, M. Piatak, J. Lifson, M. Roederer, R. Veazey, J. J. Mattapallil, α4^{+}β7^{hi}CD4^{+} memory T cells harbor most Th-17 cells and are preferentially infected during acute SIV infection. *Mucosal Immunol.* **2**, 439–449 (2009).

22. E. Martinelli, F. Veglia, D. Goode, N. Guerra-Perez, M. Aravantinou, J. Arthos, M. Piatak Jr., J. D. Lifson, J. Blanchard, A. Gettie, M. Robbiani, The frequency of α4β7^{high} memory CD4^{+} T cells correlates with susceptibility to rectal simian immunodeficiency virus infection. *J. Acquir. Immune Defic. Syndr.* **64**, 325–331 (2013).

23. A. Sivro, A. Schuetz, D. Sheward, V. Joag, S. Yegorov, L. J. Liebenberg, N. Yende-Zuma, A. Stalker, R. S. Mwatelah, P. Selhorst, N. Garrett, N. Samsunder, A. Balgobin, F. Nawaz, C. Cicala, J. Arthos, A. S. Fauci, A. O. Anzala, J. Kimani, B. S. Bagaya, N. Kiwanuka, C. Williamson, R. Kaul, J. S. Passmore, N. Phanuphak, J. Ananworanich, A. Ansari, Q. Abdool Karim, S. S. Abdool Karim, L. R. McKinnon; CAPRISA004 and RV254 study groups, Integrin α4β7 expression on peripheral blood CD4^{+} T cells predicts HIV acquisition and disease progression outcomes. *Sci. Transl. Med.* **10**, eaam6354 (2018).

24. D. Goode, R. Truong, G. Villegas, G. Calenda, N. Guerra-Perez, M. Piatak, J. D. Lifson, J. Blanchard, A. Gettie, M. Robbiani, E. Martinelli, HSV-2-driven increase in the expression of α4β7 correlates with increased susceptibility to vaginal SHIV_SF162P3 infection. *PLOS Pathog.* **10**, e1004567 (2014).

25. B. Shannon, T. J. Yi, J. Thomas-Pavanel, L. Chieza, P. Janakiram, M. Saunders, W. Tharao, S. Huibner, R. Remis, A. Rebbapragada, R. Kaul, Impact of asymptomatic herpes simplex virus type 2 infection on mucosal homing and immune cell subsets in the blood and female genital tract. *J. Immunol.* **192**, 5074–5082 (2014).

26. S. N. Byrareddy, B. Kallam, J. Arthos, C. Cicala, F. Nawaz, J. Hiatt, E. N. Kersh, J. M. McNicholl, D. Hanson, K. A. Reimann, M. Brameier, L. Walter, K. Rogers, A. E. Mayne, P. Dunbar, T. Villinger, D. Little, T. G. Parslow, P. J. Santangelo, F. Villinger, A. S. Fauci, A. A. Ansari, Targeting α4β7 integrin reduces mucosal transmission of simian immunodeficiency virus and protects gut-associated lymphoid tissue from infection. *Nat. Med.* **20**, 1397–1400 (2014).

27. S. N. Byrareddy, J. Arthos, C. Cicala, F. Villinger, K. T. Ortiz, D. Little, N. Sidell, M. A. Kane, J. Yu, J. W. Jones, P. J. Santangelo, C. Zurla, L. R. McKinnon, K. B. Arnold, C. E. Woody, L. Walter, C. Roos, A. Noll, D. Van Ryk, K. Jelicic, R. Cimbro, S. Gumber, M. D. Reid, V. Adsay, P. K. Amancha, A. E. Mayne, T. G. Parslow, A. S. Fauci, A. A. Ansari, Sustained virologic control in SIV[+] macaques after antiretroviral and α4β7 antibody therapy. *Science* **354**, 197–202 (2016).

28. B. G. Feagan, P. Rutgeerts, B. E. Sands, S. Hanauer, J.-F. Colombel, W. J. Sandborn, G. Van Assche, J. Axler, H.-J. Kim, S. Danese, I. Fox, C. Milch, S. Sankoh, T. Wyant, J. Xu, A. Parikh; GEMINI 1 Study Group, Vedolizumab as induction and maintenance therapy for ulcerative colitis. *N. Engl. J. Med.* **369**, 699–710 (2013).

29. W. J. Sandborn, B. G. Feagan, P. Rutgeerts, S. Hanauer, J.-F. Colombel, B. E. Sands, M. Lukas, R. N. Fedorak, S. Lee, B. Bressler, I. Fox, M. Rosario, S. Sankoh, J. Xu, K. Stephens, C. Milch, A. Parikh; GEMINI 1 Study Group, Vedolizumab as induction and maintenance therapy for Crohn's disease. *N. Engl. J. Med.* **369**, 711–721 (2013).

30. G. Novak, P. Hindryckx, R. Khanna, V. Jairath, B. G. Feagan, The safety of vedolizumab for the treatment of ulcerative colitis. *Expert Opin. Drug Saf.* **16**, 501–507 (2017).

31. R. Ungaro, S. Mehandru, P. B. Allen, L. Peyrin-Biroulet, J. F. Colombel, Ulcerative colitis. *Lancet* **389**, 1756–1770 (2017).

32. J. Torres, S. Mehandru, J. F. Colombel, L. Peyrin-Biroulet, Crohn's disease. *Lancet* **389**, 1741–1755 (2017).

33. P. S. Dulai, S. Singh, X. Jiang, F. Peerani, N. Narula, K. Chaudrey, D. Whitehead, D. Hudesman, D. Lukin, A. Swaminath, E. Shmidt, S. Wang, B. S. Boland, J. T. Chang, S. Kane, C. A. Siegel, E. V. Loftus, W. J. Sandborn, B. E. Sands, J.-F. Colombel, The real-world effectiveness and safety of vedolizumab for moderate-severe Crohn's disease: Results From the US VICTORY Consortium. *Am. J. Gastroenterol.* **111**, 1147–1155 (2016).

34. S. Mehandru, M. A. Poles, K. Tenner-Racz, V. Manuelli, P. Jean-Pierre, P. Lopez, A. Shet, A. Low, H. Mohri, D. Boden, P. Racz, M. Markowitz, Mechanisms of gastrointestinal CD4^{+} T-cell depletion during acute and early human immunodeficiency virus type 1 infection. *J. Virol.* **81**, 599–612 (2007).

35. R. J. Bryant, P. M. Banks, D. P. O'Malley, Ki67 staining pattern as a diagnostic tool in the evaluation of lymphoproliferative disorders. *Histopathology* **48**, 505–515 (2006).

36. K. S. Ravichandran, U. Lorenz, Engulfment of apoptotic cells: Signals for a good meal. *Nat. Rev. Immunol.* **7**, 964–974 (2007).

37. S. Mehandru, M. A. Poles, K. Tenner-Racz, P. Jean-Pierre, V. Manuelli, P. Lopez, A. Shet, A. Low, H. Mohri, D. Boden, P. Racz, M. Markowitz, Lack of mucosal immune reconstitution during prolonged treatment of acute and early HIV-1 infection. *PLOS Med.* **3**, e484 (2006).

38. E. C. Butcher, L. J. Picker, Lymphocyte homing and homeostasis. *Science* **272**, 60–66 (1996).

39. S. C. Bendall, E. F. Simonds, P. Qiu, E.-A. Amir, P. O. Krutzik, R. Finck, R. V. Bruggner, R. Melamed, A. Trejo, O. I. Ornatsky, R. S. Balderas, S. K. Plevritis, K. Sachs, D. Pe'er, S. D. Tanner, G. P. Nolan, Single-cell mass cytometry of differential immune and drug responses across a human hematopoietic continuum. *Science* **332**, 687–696 (2011).

40. S. C. Bendall, G. P. Nolan, From single cells to deep phenotypes in cancer. *Nat. Biotechnol.* **30**, 639–647 (2012).

41. E.-A. Amir, K. L. Davis, M. D. Tadmor, E. F. Simonds, J. H. Levine, S. C. Bendall, D. K. Shenfeld, S. Krishnaswamy, G. P. Nolan, D. Pe'er, viSNE enables visualization of high dimensional single-cell data and reveals phenotypic heterogeneity of leukemia. *Nat. Biotechnol.* **31**, 545–552 (2013).

42. F. Maldarelli, X. Wu, L. Su, F. R. Simonetti, W. Shao, S. Hill, J. Spindler, A. L. Ferris, J. W. Mellors, M. F. Kearney, J. M. Coffin, S. H. Hughes, HIV latency. Specific HIV integration sites are linked to clonal expansion and persistence of infected cells. *Science* **345**, 179–183 (2014).

43. J. V. Giorgi, L. E. Hultin, J. A. McKeating, T. D. Johnson, B. Owens, L. P. Jacobson, R. Shih, J. Lewis, D. J. Wiley, J. P. Phair, S. M. Wolinsky, R. Detels, Shorter survival in advanced human immunodeficiency virus type 1 infection is more closely associated with T lymphocyte activation than with plasma virus burden or virus chemokine coreceptor usage. *J. Infect. Dis.* **179**, 859–870 (1999).

44. P. W. Hunt, J. N. Martin, E. Sinclair, B. Bredt, E. Hagos, H. Lampiris, S. G. Deeks, T cell activation is associated with lower CD4^{+} T cell gains in human immunodeficiency virus-infected patients with sustained viral suppression during antiretroviral therapy. *J. Infect. Dis.* **187**, 1534–1543 (2003).

45. E. Scully, G. Alter, NK Cells in HIV Disease. *Curr. HIV/AIDS Rep.* **13**, 85–94 (2016).

46. G. Calenda, R. Keavvichit, G. Arrode-Bruses, K. Pattanapanyasat, I. Frank, S. N. Byrareddy, J. Arthos, C. Cicala, B. Grasperge, J. L. Blanchard, A. Gettie, K. A. Reimann, A. A. Ansari, E. Martinelli, Integrin α4β7 blockade preferentially impacts CCR6^{+} lymphocyte subsets in blood and mucosal tissues of naive rhesus macaques. *J. Immunol.* **200**, 810–820 (2018).

47. E. R. Fedyk, T. Wyant, L. L. Yang, V. Csizmadia, K. Burke, H. Yang, V. J. Kadambi, Exclusive antagonism of the α4β7 integrin by vedolizumab confirms the gut-selectivity of this pathway in primates. *Inflamm. Bowel Dis.* **18**, 2107–2119 (2012).

48. S. V. Kim, W. V. Xiang, C. Kwak, Y. Yang, X. W. Lin, M. Ota, U. Sarpel, D. B. Rifkin, R. Xu, D. R. Littman, GPR15-mediated homing controls immune homeostasis in the large intestine mucosa. *Science* **340**, 1456–1459 (2013).

49. K. Tenner-Racz, H. J. Stellbrink, J. van Lunzen, C. Schneider, J.-P. Jacobs, B. Raschdorff, G. Großschupff, R. M. Steinman, P. Racz, The unenlarged lymph nodes of HIV-1-infected, asymptomatic patients with high CD4 T cell counts are sites for virus replication and CD4 T cell proliferation. The impact of highly active antiretroviral therapy. *J. Exp. Med.* **187**, 949–959 (1998).

50. C. Petrovas, T. Yamamoto, M. Y. Gerner, K. L. Boswell, K. Wloka, E. C. Smith, D. R. Ambrozak, N. G. Sandler, K. J. Timmer, X. Sun, L. Pan, A. Poholek, S. S. Rao, J. M. Brenchley, S. M. Alam, G. D. Tomaras, M. Roederer, D. C. Douek, R. A. Seder,

R. N. Germain, E. K. Haddad, R. A. Koup, CD4 T follicular helper cell dynamics during SIV infection. *J. Clin. Invest.* **122**, 3281–3294 (2012).

51. B. A. Heesters, R. C. Myers, M. C. Carroll, Follicular dendritic cells: Dynamic antigen libraries. *Nat. Rev. Immunol.* **14**, 495–504 (2014).

52. A. T. Haase, K. Henry, M. Zupancic, G. Sedgewick, R. A. Faust, H. Melroe, W. Cavert, K. Gebhard, K. Staskus, Z.-Q. Zhang, P. J. Dailey, H. H. Balfour Jr., A. Erice, A. S. Perelson, Quantitative image analysis of HIV-1 infection in lymphoid tissue. *Science* **274**, 985–989 (1996).

53. B. F. Keele, L. Tazi, S. Gartner, Y. Liu, T. B. Burgon, J. D. Estes, T. C. Thacker, K. A. Crandall, J. C. McArthur, G. F. Burton, Characterization of the follicular dendritic cell reservoir of human immunodeficiency virus type 1. *J. Virol.* **82**, 5548–5561 (2008).

54. S. L. Heath, J. G. Tew, J. G. Tew, A. K. Szakal, G. F. Burton, Follicular dendritic cells and human immunodeficiency virus infectivity. *Nature* **377**, 740–744 (1995).

55. M. Perreau, A.-L. Savoye, E. De Crignis, J.-M. Corpataux, R. Cubas, E. K. Haddad, L. De Leval, C. Graziosi, G. Pantaleo, Follicular helper T cells serve as the major CD4 T cell compartment for HIV-1 infection, replication, and production. *J. Exp. Med.* **210**, 143–156 (2013).

56. S. L. Kohler, M. N. Pham, J. M. Folkvord, T. Arends, S. M. Miller, B. Miles, A. L. Meditz, M. McCarter, D. N. Levy, E. Connick, Germinal center T follicular helper cells are highly permissive to HIV-1 and alter their phenotype during virus replication. *J. Immunol.* **196**, 2711–2722 (2016).

57. T. Amet, Y. M. Son, L. Jiang, I. S. Cheon, S. Huang, S. K. Gupta, A. L. Dent, L. J. Montaner, Q. Yu, J. Sun, BCL6 represses antiviral resistance in follicular T helper cells. *J. Leukoc. Biol.* **102**, 527–536 (2017).

58. Y. Fukazawa, R. Lum, A. A. Okoye, H. Park, K. Matsuda, J. Y. Bae, S. I. Hagen, R. Shoemaker, C. Deleage, C. Lucero, D. Morcock, T. Swanson, A. W. Legasse, M. K. Axthelm, J. Hesselgesser, R. Geleziunas, V. M. Hirsch, P. T. Edlefsen, M. Piatak Jr., J. D. Estes, J. D. Lifson, L. J. Picker, B cell follicle sanctuary permits persistent productive simian immunodeficiency virus infection in elite controllers. *Nat. Med.* **21**, 132–139 (2015).

59. C. G. Vinuesa, J. G. Cyster, How T cells earn the follicular rite of passage. *Immunity* **35**, 671–680 (2011).

60. M. P. Bronnimann, P. J. Skinner, E. Connick, The B-cell follicle in HIV infection: Barrier to a cure. *Front. Immunol.* **9**, 20 (2018).

61. G. H. Mylvaganam, D. Rios, H. M. Abdelaal, S. Iyer, G. Tharp, M. Mavigner, S. Hicks, A. Chahroudi, R. Ahmed, S. E. Bosinger, I. R. Williams, P. J. Skinner, V. Velu, R. R. Amara, Dynamics of SIV-specific CXCR5+ CD8 T cells during chronic SIV infection. *Proc. Natl. Acad. Sci. U.S.A.* **114**, 1976–1981 (2017).

62. A. Pegu, M. Asokan, L. Wu, K. Wang, J. Hataye, J. P. Casazza, X. Guo, W. Shi, I. Georgiev, T. Zhou, X. Chen, S. O'Dell, J.-P. Todd, P. D. Kwong, S. S. Rao, Z.-Y. Yang, R. A. Koup, J. R. Mascola, G. J. Nabel, Activation and lysis of human CD4 cells latently infected with HIV-1. *Nat. Commun.* **6**, 8447 (2015).

63. C. K. Bullen, G. M. Laird, C. M. Durand, J. D. Siliciano, R. F. Siliciano, New ex vivo approaches distinguish effective and ineffective single agents for reversing HIV-1 latency in vivo. *Nat. Med.* **20**, 425–429 (2014).

64. T. H. Ho, R. Fausel, J. Yang, T. Swartz, J. Torres, J. Aberg, J. F. Colombe, S. Mehandru, The impact of concurrent HIV-1 infection on the management of patients with inflammatory bowel disease. *Gastroenterology* **150**, S42 (2016).

65. C. Vandergeeten, R. Fromentin, E. Merlini, M. B. Lawani, S. DaFonseca, W. Bakeman, A. McNulty, M. Ramgopal, N. Michael, J. H. Kim, J. Ananworanich, N. Chomont, Cross-clade ultrasensitive PCR-based assays to measure HIV persistence in large-cohort studies. *J. Virol.* **88**, 12385–12396 (2014).

66. F. A. Procopio, R. Fromentin, D. A. Kulpa, J. H. Brehm, A.-G. Bebin, M. C. Strain, D. D. Richman, U. O'Doherty, S. Palmer, F. M. Hecht, R. Hoh, R. J. O. Barnard, M. D. Miller, D. J. Hazuda, S. G. Deeks, R. P. Sékaly, N. Chomont, A novel assay to measure the magnitude of the inducible viral reservoir in HIV-infected individuals. *EBioMedicine* **2**, 874–883 (2015).

INFECTIOUS DISEASE

A live vaccine rapidly protects against cholera in an infant rabbit model

Troy P. Hubbard *et al.* (Matthew K. Waldor)

Outbreaks of cholera, a rapidly fatal diarrheal disease, often spread explosively. The efficacy of reactive vaccination campaigns—deploying *Vibrio cholerae* vaccines during epidemics—is partially limited by the time required for vaccine recipients to develop adaptive immunity. We created HaitiV, a live attenuated cholera vaccine candidate, by deleting diarrheagenic factors from a recent clinical isolate of *V. cholerae* and incorporating safeguards against vaccine reversion. We demonstrate that administration of HaitiV 24 hours before lethal challenge with wild-type *V. cholerae* reduced intestinal colonization by the wild-type strain, slowed disease progression, and reduced mortality in an infant rabbit model of cholera. HaitiV-mediated protection required viable vaccine, and rapid protection kinetics are not consistent with development of adaptive immunity. These features suggest that HaitiV mediates probiotic-like protection from cholera, a mechanism that is not known to be elicited by traditional vaccines. Mathematical modeling indicates that an intervention that works at the speed of HaitiV-mediated protection could improve the public health impact of reactive vaccination.

AUTOIMMUNITY

Antibody blockade of IL-15 signaling has the potential to durably reverse vitiligo

Jillian M. Richmond *et al.* (John E. Harris)

Vitiligo is an autoimmune disease of the skin mediated by CD8$^+$ T cells that kill melanocytes and create white spots. Skin lesions in vitiligo frequently return after discontinuing conventional treatments, supporting the hypothesis that autoimmune memory is formed at these locations. We found that lesional T cells in mice and humans with vitiligo display a resident memory (T_{RM}) phenotype, similar to those that provide rapid, localized protection against reinfection from skin and mucosal-tropic viruses. Interleukin-15 (IL-15)–deficient mice reportedly have impaired T_{RM} formation, and IL-15 promotes T_{RM} function ex vivo. We found that both human and mouse T_{RM} express the CD122 subunit of the IL-15 receptor and that keratinocytes up-regulate CD215, the subunit required to display the cytokine on their surface to promote activation of T cells. Targeting IL-15 signaling with an anti-CD122 antibody reverses disease in mice with established vitiligo. Short-term treatment with anti-CD122 inhibits T_{RM} production of interferon-γ (IFNγ), and long-term treatment depletes T_{RM} from skin lesions. Short-term treatment with anti-CD122 can provide durable repigmentation when administered either systemically or locally in the skin. On the basis of these data, we propose that targeting CD122 may be a highly effective and even durable treatment strategy for vitiligo and other tissue-specific autoimmune diseases involving T_{RM}.

Alloreactive fetal T cells promote uterine contractility in preterm labor via IFN-γ and TNF-α

Michela Frascoli *et al.* (Tippi C. MacKenzie)

Healthy pregnancy is the most successful form of graft tolerance, whereas preterm labor (PTL) may represent a breakdown in maternal-fetal tolerance. Although maternal immune responses have been implicated in pregnancy complications, fetal immune responses against maternal antigens are often not considered. To examine the fetal immune system in the relevant clinical setting, we analyzed maternal and cord blood in patients with PTL and healthy term controls. We report here that the cord blood of preterm infants has higher amounts of inflammatory cytokines and a greater activation of dendritic cells. Moreover, preterm cord blood is characterized by the presence of a population of central memory cells with a type 1 T helper phenotype, which is absent in term infants, and an increase in maternal microchimerism. T cells from preterm infants mount a robust proliferative, proinflammatory response to maternal antigens compared to term infants yet fail to respond to third-party antigens. Furthermore, we show that T cells from preterm infants stimulate uterine myometrial contractility through interferon-γ and tumor necrosis factor–α. In parallel, we found that adoptive transfer of activated T cells directly into mouse fetuses resulted in pregnancy loss. Our findings indicate that fetal inflammation and rejection of maternal antigens can contribute to the signaling cascade that promotes uterine contractility and that aberrant fetal immune responses should be considered in the pathogenesis of PTL.

Epigenetic immune cell counting in human blood samples for immunodiagnostics

Udo Baron *et al.* (Sven Olek)

Immune cell profiles provide valuable diagnostic information for hematologic and immunologic diseases. Although it is the most widely applied analytical approach, flow cytometry is limited to liquid blood. Moreover, either analysis must be performed with fresh samples or cell integrity needs to be guaranteed during storage and transport. We developed epigenetic real-time quantitative polymerase chain reaction (qPCR) assays for analysis of human leukocyte subpopulations. After method establishment, whole blood from 25 healthy donors and 97 HIV[+] patients as well as dried spots from 250 healthy newborns and 24 newborns with primary immunodeficiencies were analyzed. Concordance between flow cytometric and epigenetic data for neutrophils and B, natural killer, CD3^{+} T, CD8^{+} T, CD4^{+} T, and FOXP3^{+} regulatory T cells was evaluated, demonstrating substantial equivalence between epigenetic qPCR analysis and flow cytometry. Epigenetic qPCR achieves both relative and absolute quantifications. Applied to dried blood spots, epigenetic immune cell quantification was shown to identify newborns suffering from various primary immunodeficiencies. Using epigenetic qPCR not only provides a precise means for immune cell counting in fresh-frozen blood but also extends applicability to dried blood spots. This method could expand the ability for screening immune defects and facilitates diagnostics of unobservantly collected samples, for example, in underdeveloped areas, where logistics are major barriers to screening.

Science Translational Medicine | AAAS

CANCER: Eradication of spontaneous malignancy by local immunotherapy

Idit Sagiv-Barfi, Debra K. Czerwinski, Shoshana Levy, Israt S. Alam, Aaron T. Mayer, Sanjiv S. Gambhir and Ronald Levy

VASCULAR BIOLOGY: Methicillin-resistant Staphylococcus aureus causes sustained collecting lymphatic vessel dysfunction

Dennis Jones, Eelco F. J. Meijer, Cedric Blatter, Shan Liao, Ethel R. Pereira, Echoe M. Bouta, Keehoon Jung, Shan Min Chin, Peigen Huang, Lance L. Munn, Benjamin J. Vakoc, Michael Otto and Timothy P. Padera

EMERGING INFECTIONS: Zika virus–related neurotropic flaviviruses infect human placental explants and cause fetal demise in mice

Derek J. Platt, Amber M. Smith, Nitin Arora, Michael S. Diamond, Carolyn B. Coyne and Jonathan J. Miner

CANCER: The systemic response to surgery triggers the outgrowth of distant immune-controlled tumors in mouse models of dormancy

Jordan A. Krall, Ferenc Reinhardt, Oblaise A. Mercury, Diwakar R. Pattabiraman, Mary W. Brooks, Michael Dougan, Arthur W. Lambert, Brian Bierie, Hidde L. Ploegh, Stephanie K. Dougan and Robert A. Weinberg

HIV: CD32 is expressed on cells with transcriptionally active HIV but does not enrich for HIV DNA in resting T cells

Mohamed Abdel-Mohsen, Leticia Kuri-Cervantes, Judith Grau-Exposito, Adam M. Spivak, Racheal A. Nell, Costin Tomescu, Surya Kumari Vadrevu, Leila B. Giron, Carla Serra-Peinado, Meritxell Genescà, Josep Castellví, Guoxin Wu, Perla M. Del Rio Estrada, Mauricio González-Navarro, Kenneth Lynn, Colin T. King, Sai Vemula, Kara Cox, Yanmin Wan, Qingsheng Li, Karam Mounzer, Jay Kostman, Ian Frank, Mirko Paiardini, Daria Hazuda, Gustavo Reyes-Terán, Douglas Richman, Bonnie Howell, Pablo Tebas, Javier Martinez-Picado, Vicente Planelles, Maria J. Buzon, Michael R. Betts and Luis J. Montaner

AUTOIMMUNITY: Commensal orthologs of the human autoantigen Ro60 as triggers of autoimmunity in lupus

Teri M. Greiling, Carina Dehner, Xinguo Chen, Kevin Hughes, Alonso J. Iñiguez, Marco Boccitto, Daniel Zegarra Ruiz, Stephen C. Renfroe, Silvio M. Vieira, William E. Ruff, Soyeong Sim, Christina Kriegel, Julia Glanternik, Xindi Chen, Michael Girardi, Patrick Degnan, Karen H. Costenbader, Andrew L. Goodman, Sandra L. Wolin and Martin A. Kriege

FIBROSIS: PD-1 up-regulation on CD4+ T cells promotes pulmonary fibrosis through STAT3-mediated IL-17A and TGF-β1 production

Lindsay J. Celada, Jonathan A. Kropski, Jose D. Herazo-Maya, Weifeng Luo, Amy Creecy, Andrew T. Abad, Ozioma S. Chioma, Grace Lee, Natalie E. Hassell, Guzel I. Shaginurova, Yufen Wang, Joyce E. Johnson, Amy Kerrigan, Wendi R. Mason, Robert P. Baughman, Gregory D. Ayers, Gordon R. Bernard, Daniel A. Culver, Courtney G. Montgomery, Toby M. Maher, Philip L. Molyneaux, Imre Noth, Steven E. Mutsaers, Cecilia M. Prele, R. Stokes Peebles Jr., Dawn C. Newcomb, Naftali Kaminsk, Timothy S. Blackwell, Luc Van Kaer and Wonder P. Drake

MULTIPLE SCLEROSIS: GDP-$_L$-Fucose synthase is a CD4+ T cell—specific autoantigen in DRB3*02:02 patients with multiple sclerosis

Raquel Planas, Radleigh Santos, Paula Tomas-Ojer, Carolina Cruciani, Andreas Lutterotti, Wolfgang Faigle, Nicole Schaeren-Wiemers, Carmen Espejo, Herena Eixarch, Clemencia Pinilla, Roland Martin and Mireia Sospedra